

From underactuation to quasi-full actuation: Aiming at a unifying control framework for articulated soft robots

Manuel Keppler¹  | Christian Ott¹ | Alin Albu-Schäffer^{1,2}

¹Institute of Robotics and Mechatronics,
German Aerospace Center (DLR),
Oberpfaffenhofen, Germany

²Department of Informatics, Technical
University Munich (TUM), Munich,
Germany

Correspondence

Manuel Keppler, Institute of Robotics and
Mechatronics, German Aerospace Center
(DLR), 82234 Oberpfaffenhofen, Germany
Email: manuel.keppler@dlr.de

Abstract

We establish a structure preserving state and input transformation that allows a class of underactuated Euler Lagrange systems to be treated as “quasi-fully” actuated. In this equivalent quasi-fully actuated form, the system is characterized by the same Lagrangian structure as the original one. This facilitates the design of control approaches that take into account the underlying physics of the system and that shape the system dynamics to a minimum extent. Due to smoothness constraints on the new input vector that acts directly on the noncollocated coordinates, we coin the term quasi-fully actuated. The class of Euler–Lagrange systems we consider is the class of articulated soft robots with nonlinear spring characteristics that are modeled with a block diagonal inertia matrix. We illustrate how the quasi-fully actuated form enables the direct transfer of control concepts that have been derived for fully actuated manipulators. We adopt the popular energy-shaping and two passivity-based concepts. The exemplary adoptions of the PD+ and Slotine and Li controllers allow us to solve the task-space tracking problem for highly elastic joint robots with nonlinear spring characteristics. These control schemes allow compliant behavior of the robot’s TCP to be specified with respect to a reference trajectory. A key aspect of the presented framework is that it enables the adoption of rigid joint controllers as well as concepts underlying the original stability analysis. We believe that our framework presents an important step toward unifying the control design for rigid and articulated soft robots.

KEY WORDS

robot control, joint elasticity, passivity-based control, impedance control, underactuated system

1 | INTRODUCTION

In recent years, we have seen significant advances in the field of robotics and an ever-increasing surge of its economic potential. Against this backdrop, development of robot manipulators with challenging nonlinear dynamics has fueled research in nonlinear control theory. This renewed research led to the development of fundamental concepts such as computed torque control,¹ energy-shaping control,² (task-space) impedance control,³ passivity-based control (PBC).^{4–6} However, the more recent development of extremely light weight robot arms with load-weight ratios comparable to the

This is an open access article under the terms of the Creative Commons Attribution License, which permits use, distribution and reproduction in any medium, provided the original work is properly cited.

© 2022 The Authors. *International Journal of Robust and Nonlinear Control* published by John Wiley & Sons Ltd.

human arm, introduced new challenges in the design of nonlinear feedback control. These manipulators were designed to enable compliant manipulation in contact with unknown environments and safe interaction with humans.^{7,8} A major challenge inherent in the control design of such lightweight robots is the flexibility that is introduced into the robot joints. The system is underactuated, since the number of degrees of freedom is twice the number of actuators and the matching property between control actions and outputs is lost (noncollocation problem). The situation became worse with the advent of robots with series elastic actuators (SEA)^{9,10} or variable impedance actuators (VIA).^{11,12} In these articulated soft robots (ASRs), one deliberately incorporates highly compliant elements into the drive train with a stiffness that is low enough that these elements can be exploited as energy storage.

In this article, we propose a control framework based on an Euler–Lagrange structure preserving state and input transformation that allows this major challenge to be circumvented. This type of control framework allows these underactuated systems to be treated as *quasi-fully actuated* (QFA), thereby literally opening the door for direct transfer from the rich pool of classical control methods for rigid robots. In this regard, the framework can be considered a step toward unifying the control design for rigid and ASRs. We call this form “quasi-fully” actuated since the new control input, on the formally noncollocated output, must be sufficiently smooth (twice differentiable with respect to time). This constraint is imposed by physics and not by the framework itself.

In the past, other concepts have been proposed to extend rigid joint controllers to the flexible joint case that rely on the singular perturbation theory¹³ or cascaded closed-loop structures.¹⁴ These concepts have in common that they introduce an inner feedback loop that provides the interface to the rigid robot controller (outer feedback loop). The singular perturbed control (SPC) method is build around Tikhonov’s theorem¹⁵ whose applicability requires a sufficiently high joint stiffness. This renders SPC methods inapplicable for highly compliant (soft) robots. Furthermore, implementing the inner loop requires, in both cases, the cancelation of nonlinear terms and additional knowledge of external forces in case of cascaded approaches. Unfortunately, nonlinearity cancelation-based schemes suffer from an intrinsic lack of robustness.¹⁶ The application of feedback linearization-based techniques on robots with compliant joints has been extensively treated by several researchers in its original formulation^{17–20} or in the revised version, in which the inertial coupling between the links and motors is considered.²¹ By canceling all nonlinearities, this technique allows a desired behavior to be imposed on the robot in a decoupled way. The two key novelties of the presented concept are: (1) This concept does not rely on an inner feedback loop to provide an interface to classical control methods for rigid robots (2) the underlying input and state transformation preserves the Euler–Lagrange structure, which facilitates adoption of control approaches that take into account the underlying physics of the system and shape it to a minimum extent. See Reference 22 for an interesting discussion on the dynamics shaping of compliant systems. The works^{23,24} use the equivalence principle to derive control laws that combine cancelation of gravity effects with motor-side PD terms to achieve set-point regulation. Using the presented framework to just cancel the effect of gravity produces a controller equal to References 23 and 24. The methods of “controlled Lagrangian”^{25,26} and IDA-PBC²⁷ transform a given Euler–Lagrange (respectively Hamiltonian) system into another Euler–Lagrange (respectively Hamiltonian) system. In this respect,^{25–27} share the Euler–Lagrange (respectively Hamiltonian) structure preserving property of the presented framework. A fundamental difference between these methods and the proposed one is that in this work the target Euler–Lagrange dynamics is characterized by kinetic and potential energies which are formulated in terms of virtual coordinates. It is worth noting that the transforming equations relating the virtual and actual coordinate do not belong to the class of points transformations*.

As we have learned from hands-on experiences in the lab, the benefit of having closed-loop dynamics that exhibit a physically intuitive form can hardly be overestimated. It provides valuable intuition during the controller tuning stage, thus significantly simplifying the controller commissioning. In particular, it allows for an intuitive feeling regarding to what extend the controller shapes the system dynamics, thereby allowing gain limits that are likely feasible in practice to be narrowed down. In addition, techniques that do not require cancelation of nonlinearities yield control designs with enhanced robustness properties. For these reasons, we decided to showcase the adoption procedure on the basis of three inspiring rigid joint controllers that evolved from fundamental physical considerations: (1) the energy-shaping concept developed by Takegaki and Arimoto,² (2) the PD+ controller,^{4,5} and (3) the Slotine and Li controller⁶ (nonadaptive version). The implementation of these concepts require full state feedback. The proposed framework itself does not impose any upper or lower bounds on the gains of the adopted rigid-robot controllers. Further, the framework allows for a smooth transition to the ‘almost rigid’ manipulator case. That is, when the joint stiffness values take infinitely large values we obtain the “rigid” control laws and no high-gain designs. See Reference 16 for an in-depth discussion of this aspect.

The layout of the article is as follows: Section 1.2 specifies the class of systems under consideration. Section 2 motivates the approach on the basis of a single robot joint and concludes with an exemplary adoption of the energy-shaping concept by Takegaki.² In Section 3, we extend the concept to the general case of a compliant robotic arm with nonlinear joint

stiffness characteristics. Section 4 demonstrates the adoption of the energy-shaping control from Takegaki.² Section 5 presents the adoption of the PD+ and Slotine and Li controller. Section 6 provides a stability analysis. Section 7 offers simulation results and brief concluding remarks.

The focus of this article is set on the fundamental aspects of the proposed framework. Extensive experimental results can be found in our previous works.^{28–31} All these passivity-based concepts can be unified and elegantly expressed in the presented framework.

1.1 | Euler–Lagrange systems

It is well known that systems described by Euler–Lagrange equations (EL) posses nice passivity properties that follow directly from energy flow considerations, see for example, Reference 32. In particular, elastic joint robots define a passive operator from applied actuator torques to motor shaft velocities, though it is not passive with respect to the link velocities. Throughout this text we describe dynamic systems with generalized coordinates $\mathbf{q} \in \mathbb{R}^{2n}$ by the EL equations

$$\frac{d}{dt} \left(\frac{\partial \mathcal{L}}{\partial \dot{\mathbf{q}}}(\mathbf{q}, \dot{\mathbf{q}}) \right) - \frac{\partial \mathcal{L}}{\partial \mathbf{q}}(\mathbf{q}, \dot{\mathbf{q}}) = \mathcal{N}\mathbf{u} - \frac{\partial \mathcal{F}}{\partial \dot{\mathbf{q}}}(\dot{\mathbf{q}}) + \mathcal{Q}_{\text{ext}}, \quad (1)$$

where $\mathcal{L}(\mathbf{q}, \dot{\mathbf{q}}) \triangleq \mathcal{T}(\mathbf{q}, \dot{\mathbf{q}}) - \mathcal{V}(\mathbf{q})$ is the Lagrangian with \mathcal{T} and \mathcal{V} representing the kinetic and potential energies, respectively. The input matrix is denoted by \mathcal{N} . We consider three types of external forces: control actions \mathbf{u} , interaction of the system with its environment $\mathcal{Q}_{\text{ext}} \in \mathbb{R}^{2n}$ and dissipation. The dissipative force $-\frac{\partial \mathcal{F}}{\partial \dot{\mathbf{q}}}(\dot{\mathbf{q}})$ is derived from a Rayleigh dissipation function $\mathcal{F}(\dot{\mathbf{q}})$ satisfying by definition

$$\dot{\mathbf{q}}^T \frac{\partial \mathcal{F}}{\partial \dot{\mathbf{q}}} \geq 0 \quad \forall \dot{\mathbf{q}} \in \mathbb{R}^n.$$

In summary, we can characterize the EL equations (1) by the EL parameters $\{\mathcal{T}(\mathbf{q}, \dot{\mathbf{q}}), \mathcal{V}(\mathbf{q}), \mathcal{F}(\dot{\mathbf{q}}), \mathcal{N}, \mathcal{Q}_{\text{ext}}\}$. Throughout this text, we denote the total energy by $\mathcal{H} \triangleq \mathcal{T} + \mathcal{V}$. The notation is inspired by the work.³³

1.2 | Dynamics of articulated soft robots

In this article, we consider ASRs which are a class of underactuated EL systems. Let $\mathbf{q} \triangleq [\mathbf{q}_u^T, \mathbf{q}_a^T]^T$ be the vector of generalized states with $\mathbf{q}_u, \mathbf{q}_a \in \mathbb{R}^n$ being the unactuated link and actuated motor states, respectively. We assume that the angular part of the kinetic energy of each rotor is mainly due to its own rotation. In this case, we can consider the model proposed by Spong.¹⁷ The kinetic and potential energies are given by

$$\mathcal{T}(\mathbf{q}_u, \dot{\mathbf{q}}) \triangleq \frac{1}{2} \dot{\mathbf{q}}^T \mathcal{M}(\mathbf{q}_u) \dot{\mathbf{q}}, \quad \mathcal{V}(\mathbf{q}) \triangleq \mathcal{V}_g(\mathbf{q}_u) + \mathcal{V}_e(\mathbf{q}_u - \mathbf{q}_a), \quad (2)$$

where \mathcal{V}_g and \mathcal{V}_e are the gravitational and elastic potential functions, $\mathcal{M} \in \mathbb{R}^{2n \times 2n}$ is the generalized inertia matrix satisfying $\mathcal{M}(\mathbf{q}_u) = \mathcal{M}^T(\mathbf{q}_u) > 0$, and $\mathcal{C} \in \mathbb{R}^{2n \times 2n}$ represents the Coriolis and centrifugal matrix. These two matrices are of the form

$$\mathcal{M}(\mathbf{q}) \triangleq \begin{bmatrix} \mathbf{M}(\mathbf{q}_u) & \mathbf{0} \\ \mathbf{0} & \mathbf{B} \end{bmatrix}; \quad \mathcal{C}(\mathbf{q}, \dot{\mathbf{q}}) \triangleq \begin{bmatrix} \mathcal{C}(\mathbf{q}_u, \dot{\mathbf{q}}_u) & \mathbf{0} \\ \mathbf{0} & \mathbf{0} \end{bmatrix},$$

and satisfy the skew-symmetry property

$$\mathbf{y}^T (\dot{\mathcal{M}}(\mathbf{q}_u) - 2\mathcal{C}(\mathbf{q}_u, \dot{\mathbf{q}}_u)) \mathbf{y} = 0, \quad \forall \mathbf{y} \in \mathbb{R}^{2n}. \quad (3)$$

Matrix $\mathbf{M}(\mathbf{q}_u)$ is the robot inertia matrix, \mathbf{B} is a diagonal matrix of actuator inertias reflected to the link side and $\mathcal{C}(\mathbf{q}_u, \dot{\mathbf{q}}_u)$ is the robot Coriolis/centrifugal matrix. Let $\mathcal{V}_e : \mathbb{R}^n \rightarrow \mathbb{R}^+$ be the elastic potential energy and $\boldsymbol{\varphi} \triangleq \mathbf{q}_a - \mathbf{q}_u$ the vector of generalized joint deflections. The generalized elastic forces that couple the motor with the link inertias are

$$\boldsymbol{\tau}(\boldsymbol{\varphi}) \triangleq \frac{\partial \mathcal{V}_e(\boldsymbol{\varphi})}{\partial \boldsymbol{\varphi}}.$$

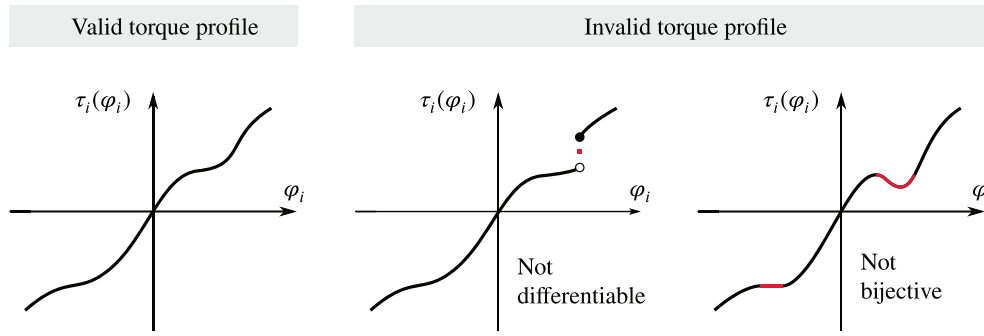


FIGURE 1 Examples of torque characteristics that satisfy and violate the assumption on the elastic potential energy. Only the first function represents a diffeomorphism

Assumption 1 summarizes the elastic potential properties.

Assumption 1. Let $\mathcal{V}_e : \mathbb{R}^n \rightarrow \mathbb{R}$ be a potential function that is at least three times continuously differentiable and let the generalized elastic forces be given by its gradient $\tau : \mathbb{R}^n \rightarrow \mathbb{R}^n$. The potential function is of such form that the component functions τ_i represent a diffeomorphism that is at least twice continuously differentiable. Moreover, the generalized elastic forces, τ_i , are strictly monotonic in their arguments with $\tau_i(0) = 0$.

Loosely speaking, the assumption above ensures that each of the n components τ_i of the generalized elastic force is a strictly monotonic function in its argument. This is true, for example, for any spring whose restoring force increases strictly monotonic with increasing deflection, as indicated in Figure 1. The local stiffness is given by the Hessian

$$\tau_{\varphi}(\varphi_0) \triangleq \left. \frac{\partial \tau(\varphi)}{\partial \varphi} \right|_{\varphi=\varphi_0} = \left. \frac{\partial^2 \mathcal{V}_e(\varphi)}{\partial \varphi^2} \right|_{\varphi=\varphi_0}.$$

In the case of linear springs, the generalized elastic forces are of the form $\tau(\varphi) = \mathbf{K}\varphi$ where the matrix $\mathbf{K} \in \mathbb{R}^{n \times n}$ is diagonal, positive definite and contains the joint stiffness coefficients. By applying Hamilton's principle, we obtain the model of a flexible joint robot

$$\Sigma_q : \mathcal{M}(\mathbf{q}_u)\ddot{\mathbf{q}} + \mathcal{C}(\mathbf{q}_u, \dot{\mathbf{q}}_u)\dot{\mathbf{q}} + \boldsymbol{\psi}(\mathbf{q}) = \mathcal{N}\mathbf{u} + \mathcal{Q}_{\text{ext}}, \quad (4)$$

with the potential forces

$$\boldsymbol{\psi}(\mathbf{q}) \triangleq \frac{\partial \mathcal{V}(\mathbf{q})}{\partial \mathbf{q}} = \begin{bmatrix} \mathbf{g}(\mathbf{q}_u) - \tau(\mathbf{q}_a - \mathbf{q}_u) \\ \tau(\mathbf{q}_a - \mathbf{q}_u) \end{bmatrix}. \quad (5)$$

System (4) is uniquely characterized by the EL parameters $\{\mathcal{T}(\mathbf{q}_u, \dot{\mathbf{q}}), \mathcal{V}(\mathbf{q}), 0, \mathcal{N}, \mathcal{Q}_{\text{ext}}\}$ with input matrix $\mathcal{N} \triangleq \begin{bmatrix} \mathbf{0} & \mathbf{0} \\ \mathbf{0} & \mathbf{I} \end{bmatrix}$ of rank n . Clearly, the system is under-actuated. By suitably partitioning the input vector, we may write $\mathbf{u} \triangleq [\mathbf{u}_1^T \quad \mathbf{u}_2^T]^T$ with $\mathbf{u}_1, \mathbf{u}_2 \in \mathbb{R}^n$ and for the external forces in analogous fashion $\mathcal{Q}_{\text{ext}} \triangleq [\mathcal{Q}_{\text{ext},1}^T, \mathcal{Q}_{\text{ext},2}^T]^T$.

We assume the existence of a C^3 forward kinematics mapping $\mathbf{h}_1 : \mathcal{D}_{q_u} \rightarrow \mathcal{D}_y$ from the link configuration variables $\mathbf{q}_u \in \mathcal{D}_{q_u} \subseteq \mathbb{R}^n$ to the task coordinates $\mathbf{y} \in \mathcal{D}_y \subseteq \mathbb{R}^m$, which, for example, describes the position and orientation of the robot end-effector, that is,

$$\mathbf{y} = \mathbf{h}_1(\mathbf{q}_u). \quad (6)$$

Throughout this article, we assume that the manipulator is nonredundant (i.e., $m = n$) and that singular configurations are avoided employing appropriate singularity avoidance strategies. Thus, the Jacobian matrix of the mapping (6)

$$\mathbf{J}(\mathbf{q}_u) = \frac{\partial \mathbf{h}_1(\mathbf{q}_u)}{\partial \mathbf{q}_u} \quad (7)$$

is nonsingular for all $\mathbf{q}_u \in \mathcal{D}_{q_u}$. Therefore, \mathbf{q}_u and \mathbf{y} are equivalent representations of the rigid robot configuration.

2 | FROM UNDERACTUATION TO QUASI-FULL ACTUATION

This section introduces the fundamental line of thoughts that lead to the state and input transformation that yields the desired quasi-fully actuated form. We introduce these thoughts on the basis of a single joint.

2.1 | A physical point of view

The proposed approach has strong connections to passivity-based methods,¹³ which exploit the robot's intrinsic physical structure. This lies at the core of our idea; we exploit the physical structure of compliant robots to transform them into an easier manageable (controllable) form. This transformation is led by energy considerations as we aim to preserve the Euler–Lagrange system structure. To sharpen the objective and provide an intuitive idea, we start with a basic example.

Before continuing, let us first review some fundamental properties of Euler–Lagrange (EL) systems. The equilibria of an EL system are determined by the critical points of its potential function. Importantly, given that the potential function has a global and unique minimum, the equilibrium of the EL system is unique and globally stable.³³ If suitable[†] damping is present in the system, this equilibrium is asymptotically stable, see Proposition 3. These two fundamental properties were first exploited in Reference 2. Takegaki and Arimoto translated the problem of point regulation of robots into a problem of shaping their potential energy and injecting damping. It can be interpreted as a two-stage approach. First, the potential energy is modified such that the system has a global and unique minimum at the desired equilibrium configuration. Second, the Rayleigh dissipation function is modified to ensure asymptotic convergence.

2.2 | A rigid joint

Let's revise the energy-shaping concept from Takegaki and Arimoto² on the basis of a single robot joint as shown in Figure 2(left). Without loss of generality, we consider the link to be of unit length. Let q be a generalized coordinate representing the link position. The total energy of the system is

$$\mathcal{H} = \underbrace{\frac{1}{2}m\dot{q}^2}_{\mathcal{T}(q,\dot{q})} + \underbrace{mg(1 - \cos q)}_{\mathcal{V}(q)}. \quad (8)$$

The control input applied to the link is denoted by u . The corresponding EL equation is

$$m\ddot{q} + g(q) = u, \quad (9)$$

where $g(q)$ is the gravitational force derived from the gravitational potential \mathcal{V} , that is, $g(q) \triangleq \frac{\partial \mathcal{V}}{\partial q}(q)$. Our goal is to asymptotically stabilize the joint at a constant equilibrium $[q, \dot{q}]^T = [q_d, 0]^T$, where q_d is the desired equilibrium link position. To this end, we modify the potential energy and Rayleigh function of the system accordingly, while leaving the kinetic energy unchanged. Since we know that a minimum of the potential energy corresponds to a stable equilibrium point, our new potential function \mathcal{V}_d should have a minimum at $q = q_d$. A basic candidate satisfying this condition is

$$\mathcal{V}_d = \frac{1}{2}k_p\tilde{q}^2, \quad (10)$$

where $\tilde{q} \triangleq q - q_d$ and $k_p > 0$. In order to render the equilibrium point attractive, we choose a Rayleigh dissipation function of the form $\mathcal{F}_d(\dot{q}) = \frac{1}{2}k_v\dot{q}^2$, $k_v > 0$. That is, we aim for an EL system with EL parameters $\{\mathcal{T}(q, \dot{q}), \mathcal{V}_d(q), \mathcal{F}_d\}$, that is, its total energy shall be given by

$$\mathcal{H}_{PD+} = \underbrace{\frac{1}{2}ml^2\dot{q}^2}_{\mathcal{T}(q,\dot{q})} + \underbrace{\frac{1}{2}k_p\tilde{q}^2}_{\mathcal{V}_d(q)}. \quad (11)$$

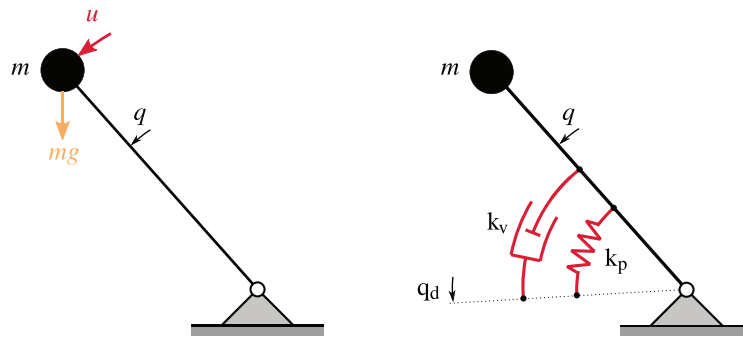


FIGURE 2 (Left) A rigid joint with control input u . The point mass m on a massless rod of unit length reflects the link inertia. (Right) A single joint under PD plus gravity compensation control

Figure 2(right) shows a visual representation of a system corresponding to \mathcal{H}_d . We can easily find a control input for system (9) such that its potential function turns into the desired one. This goal can be achieved by

$$u_{\text{PD+}} = - \underbrace{\frac{\partial V_c(q)}{\partial q}}_{\text{energy-shaping}} - \underbrace{\frac{\partial \mathcal{F}_d(\dot{q})}{\partial \dot{q}}}_{\text{damping injection}} = g(q) - k_p \tilde{q} - k_v \dot{q}. \quad (12)$$

with the potential function

$$\mathcal{V}_c(q) \triangleq \mathcal{V}_d(q) - \mathcal{V}(q) \quad (13)$$

that can be considered as the potential of the controller.³³ Equation (12) represents the popular PD plus gravity compensation control law. In addition to full-state measurement, this method relies on the fact that the system is fully actuated. Applying control input (12) to system (9), we get the closed-loop model

$$m\ddot{q} + k_v \dot{q} + k_p \tilde{q} = 0, \quad (14)$$

for which the total energy is the desired Hamiltonian $\mathcal{H}_{\text{PD+}}$ from (11).

2.3 | A series elastic joint

How can we transfer this idea to ASRs? We start with some initial observations for a single compliant joint as shown in Figure 3(left).

The value of the illustration in Figure 3(left) manifests in the fact that it equips us with a simple and physically intuitive picture for all the considerations that are about to come. Let q_u and q_a be the unactuated link and actuated motor positions, and

$$\varphi \triangleq q_a - q_u \quad (15)$$

the joint deflection. We consider q_u as the (noncollocated) output. The link and motor inertias are represented by the point masses m and b that are attached to massless links. Again, w.l.o.g. we assume links of unit length. The joint stiffness is denoted by k . The total energy of the system is

$$\mathcal{H}(q_u, q_a, \dot{q}_u, \dot{q}_a) = \underbrace{\frac{1}{2} (m\dot{q}_u^2 + b\dot{q}_a^2)}_{\mathcal{T}(\dot{q}_u, \dot{q}_a)} + \underbrace{\frac{1}{2} k(q_a - q_u)^2 + mg(1 - \cos q_u)}_{\mathcal{V}(q_u, q_a)} \quad (16)$$

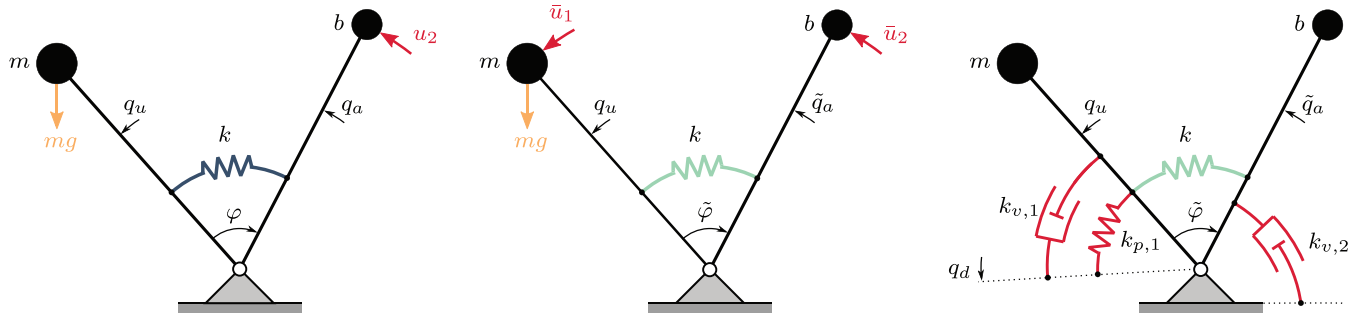


FIGURE 3 (Left) An elastic joint with point masses m and b on massless rods representing the reflected link and motor inertias, respectively. The control input u_2 acts on the motor inertia. (Mid) The quasi-fully actuated system with the new inputs \bar{u}_1 and \bar{u}_2 . (Right) A single elastic joint under adopted PD plus gravity compensation control

with \mathcal{V} being the sum of the elastic, \mathcal{V}_e , and gravitational, \mathcal{V}_g , potential energies. Its EL parameters are $\{\mathcal{T}(\dot{q}_u, \dot{q}_a), \mathcal{V}(q_u, q_a), 0, \mathcal{N}, Q_{\text{ext}}\}$ with the input matrix $\mathcal{N} \triangleq \begin{bmatrix} 0 & 0 \\ 0 & 1 \end{bmatrix}$ and the input vector $\mathbf{u} = [u_1, u_2]^T$. Let $Q_{\text{ext}} = [Q_{\text{ext},1}, Q_{\text{ext},2}]$ be the vector of external forces, then the model is given by the EL equations

$$\Sigma_0 : \begin{bmatrix} m & 0 \\ 0 & b \end{bmatrix} \begin{bmatrix} \ddot{q}_u \\ \ddot{q}_a \end{bmatrix} + \begin{bmatrix} k & -k \\ -k & k \end{bmatrix} \begin{bmatrix} q_u \\ q_a \end{bmatrix} + \begin{bmatrix} g(q_u) \\ 0 \end{bmatrix} = \begin{bmatrix} 0 \\ u_2 \end{bmatrix} + Q_{\text{ext}}. \quad (17)$$

Now imagine that we had a control input \bar{u}_1 that acts directly on the link of system (17). This would trivialize the energy shaping and damping injection procedure. Introducing the generalized force

$$\tau(\varphi) \triangleq \frac{\partial \mathcal{V}_e(\varphi)}{\partial \varphi} = k\varphi, \quad (18)$$

we can express the error between the actual and desired joint force—analogously to (18)—in terms of a generalized force

$$\tau(\tilde{\varphi}) \triangleq \tau(\varphi) - \bar{u}_1, \quad (19)$$

where $\tilde{\varphi}$ represents a *virtual joint* deflection encoding the force error, as visualized in Figure 4. This is the fundamental idea underlying this work; we encode the force error by a virtual joint deflection. The central theme of *duality* is well established in physics and mathematics. In mechanics, many terms are associated into pairs called duals, for example, force (stress) and deformation (strain).³⁵ Here, we introduce a duality between the force error and a virtual deflection. Using the definition (18), we can rewrite (19)

$$\tilde{\varphi} = \varphi - k^{-1}\bar{u}_1. \quad (20)$$

Remark 1. In (19) we are not limited to choosing the same potential function, \mathcal{V}_e , for encoding the force error. However, in this work, our goal is to transform the underactuated dynamics into a quasi-fully actuated form that preserves the Euler–Lagrange structure. For this reason, we choose again potential function \mathcal{V}_e .

Introducing new motor coordinates $\tilde{q}_a \triangleq \tilde{\varphi} + q_u$, in analogous form to (15), we can reformulate (20) in terms of motor coordinates

$$\tilde{q}_a = q_a - k^{-1}\bar{u}_1. \quad (21)$$

Geometrically, the new motor state is formed by shifting the original motor position. The magnitude of the shift is directly proportional to the desired torque \bar{u}_1 with the joint compliance k^{-1} being the coefficient of proportionality. Noting that (21) has the same form as (20), it is clear that Figure 4 serves as visualization of (21) as well (simply replace the deflection

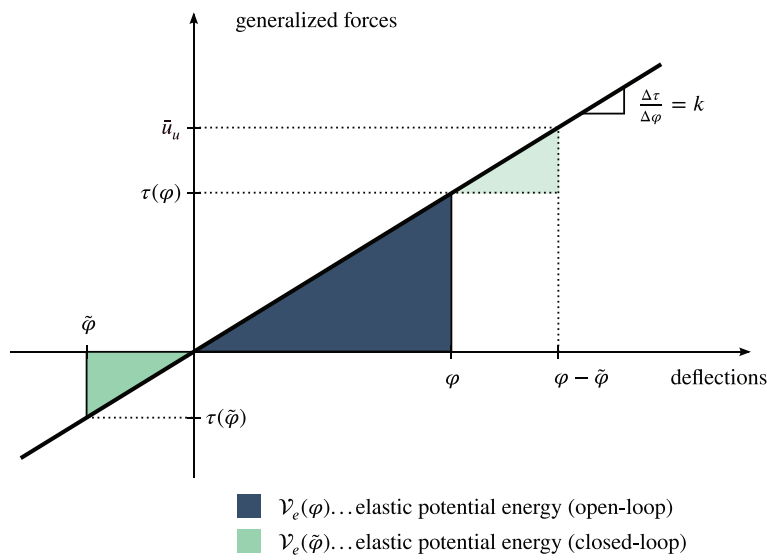


FIGURE 4 State transformations for linear springs: deflection states

coordinates with the corresponding motor coordinates). Inspired by Keppler et al.,³⁰ we use relation (21), to perform a state transformation $[q_u, q_a] \mapsto [\bar{q}_u, \tilde{q}_a]$ for system (17). Applying

$$\begin{bmatrix} q_u \\ q_a \end{bmatrix} = \begin{bmatrix} 1 & 0 \\ 0 & 1 \end{bmatrix} \begin{bmatrix} \bar{q}_u \\ \tilde{q}_a \end{bmatrix} + \begin{bmatrix} 0 \\ k^{-1}\bar{u}_1 \end{bmatrix} \quad (22)$$

to (17) yields

$$\begin{bmatrix} m & 0 \\ 0 & b \end{bmatrix} \begin{bmatrix} \ddot{q}_u \\ \ddot{\tilde{q}}_a \end{bmatrix} + \begin{bmatrix} k & -k \\ -k & k \end{bmatrix} \begin{bmatrix} q_u \\ \tilde{q}_a \end{bmatrix} + \begin{bmatrix} g(q_u) \\ 0 \end{bmatrix} = \begin{bmatrix} \bar{u}_1 \\ 0 \end{bmatrix} - \begin{bmatrix} 0 \\ \gamma \end{bmatrix} + Q_{\text{ext}} \quad (23)$$

with $\gamma \triangleq \bar{u}_1 + bk^{-1}\ddot{u}_1$. Substituting the input transformation

$$u_2 = \bar{u}_2 + \bar{u}_1 + bk^{-1}\ddot{u}_1, \quad (24)$$

into (23) gives the “quasi-fully” actuated form as visualized in Figure 3(mid)

$$\Sigma_1 : \begin{bmatrix} m & 0 \\ 0 & b \end{bmatrix} \begin{bmatrix} \ddot{q}_u \\ \ddot{\tilde{q}}_a \end{bmatrix} + \begin{bmatrix} k & -k \\ -k & k \end{bmatrix} \begin{bmatrix} q_u \\ \tilde{q}_a \end{bmatrix} + \begin{bmatrix} g(q_u) \\ 0 \end{bmatrix} = \begin{bmatrix} \bar{u}_1 \\ \bar{u}_2 \end{bmatrix} + Q_{\text{ext}}. \quad (25)$$

Strikingly, by considering q_u and \tilde{q}_a as generalized coordinates, system (25) represents an EL system with total energy

$$\mathcal{H}(q_u, \tilde{q}_a, \dot{q}_u, \dot{\tilde{q}}_a) = \underbrace{\frac{1}{2} \left(m\dot{q}_u^2 + b\dot{\tilde{q}}_a^2 \right)}_{\mathcal{T}(\dot{q}_u, \dot{\tilde{q}}_a)} + \underbrace{\frac{1}{2}k(\tilde{q}_a - q_u)^2}_{\mathcal{V}(q_u, \tilde{q}_a)} + \mathcal{V}_g(q_u),$$

The EL parameters are $\{\mathcal{T}(\dot{q}_u, \dot{\tilde{q}}_a), \mathcal{V}(q_u, \tilde{q}_a), 0, \mathcal{N}_1\}$ with an identity input matrix $\mathcal{N}_1 \triangleq \mathbf{I} \in \mathbb{R}^2$, and the new control vector is $\bar{\mathbf{u}} \triangleq [\bar{u}_1 \ \bar{u}_2]^T$. In summary, we have transformed the feedback stabilization problem of an underactuated EL system into a feedback stabilization problem of a quasi-fully-actuated EL system with the *same* EL parameters. Obviously, the input matrix is not the same, but the system dynamics is characterized by the same kinetic and potential energy functions. Clearly, the passivity properties are preserved and system Σ_1 defines a passive map $\bar{\mathbf{u}} + Q_{\text{ext}} \mapsto [\dot{q}_u \ \dot{\tilde{q}}_a]^T$. This can be easily shown with \mathcal{H} as storage function.

It is important to point out that our new link-side control input \bar{u}_1 obeys some restrictions. From the input transformation (24), it is clear that it must be twice differentiable with respect to time. In addition, we must ensure that (19) defines a diffeomorphism between the original deflection state φ and the new deflection state $\tilde{\varphi}$. In order to simplify the analysis, we assume that \bar{u}_1 is solely a function of q_u , \dot{q}_u and t . Further, we assume that \bar{u}_1 is a bounded function for bounded q_u , \dot{q}_u and for any $t \in [0, \infty)$. As we will see in the next step, these constraints pose no limitation in our goal of adopting the energy-shaping technique to solve the regulation problem.

Remark 2. For the case $\bar{u}_1 = 0$, it follows from (21) that $q_a = \tilde{q}_a$, and thus system Σ_0 and Σ_1 are equivalent. In other words, as long as we do not pick a control law for \bar{u}_1 the process so far does not change the intrinsic system dynamics at all. Thus we refer to (24) as an input transformation. Only in the second stage, when designing \bar{u}_1 and \bar{u}_2 , we will actually shape the system dynamics.

Considering the quasi-fully actuated system, we could now proceed with applying classical energy-shaping and damping injection techniques that have been developed for fully actuated systems such as References 2,4,6,36. However, it will be rewarding to exploit the duality of the force error and the new deflection state that we introduced in (20). Thus, let us perform a change of coordinates from the virtual motor space into the virtual deflection space. This allows us to exploit the central force field character of the elastic potential to simplify any analysis further down the road. As demonstrated below, this step separates the potential forces in rigid body and elastic potential forces. This point is critical for analyzing and controlling the robot arm with respect to the dynamic behavior of its end-effector (the unified force and motion control problem in task space). We treat this problem in Section 5. Applying the coordinate transformation $[q_u, \tilde{q}_a] \mapsto [q_u, \tilde{\varphi}]$ with

$$\begin{bmatrix} q_u \\ \tilde{\varphi} \end{bmatrix} = T_2 \begin{bmatrix} q_u \\ \tilde{q}_a \end{bmatrix}, \quad T_2 \triangleq \begin{bmatrix} 1 & 0 \\ -1 & 1 \end{bmatrix} \quad (26)$$

to system (25), we get for the transformed Hamiltonian

$$\mathcal{H}(q_u, q_u + \tilde{\varphi}, \dot{q}_u, \dot{q}_u + \dot{\tilde{\varphi}}) = \underbrace{\frac{1}{2} (m\dot{q}_u^2 + b(\dot{q}_u + \dot{\tilde{\varphi}})^2)}_{\mathcal{T}(\dot{q}_u, \dot{q}_u + \dot{\tilde{\varphi}})} + \underbrace{\frac{1}{2} k\tilde{\varphi}^2}_{\mathcal{V}_e(\tilde{\varphi})} + \mathcal{V}_g(q_u). \quad (27)$$

We can think of this transformation as a separation of the generalized coordinates into rigid and elastic coordinates. We observe that the total potential energy is a superposition of the rigid body and elastic potential energies. The new EL parameters are $\{\mathcal{T}(\dot{q}_u, \dot{q}_u + \dot{\tilde{\varphi}}), \mathcal{V}(q_u, q_u + \tilde{\varphi}), 0, \mathcal{N}_2\}$. Notice that only the input matrix has changed to $\mathcal{N}_2 \triangleq T_2^{-T} \mathcal{N}_1 = \begin{bmatrix} 1 & 1 \\ 0 & 1 \end{bmatrix}$. Applying Hamilton's principle to (27), we get the first EL equation

$$\frac{d}{dt} \left(\frac{\partial \mathcal{L}}{\partial \dot{q}_u} \right) = -g(q_u) + \sum_{i=1}^2 (\bar{u}_i + Q_{\text{ext},i}). \quad (28)$$

When performing a change of coordinates the virtual work of the generalized forces must be conserved which gives us the last two terms in (28). It is clear that in order to (asymptotically) stabilize the output at a desired position, it is sufficient to rely on feedback of q_u, \dot{q}_u only in \bar{u}_1 . We could easily cancel the effect of the gravity field by choosing our rigid input \bar{u}_1 accordingly. In this case, the potential function would be independent of the output q_u which would trivialize the energy-shaping part of the controller design. The second EL equation is

$$\frac{d}{dt} \left(\frac{\partial \mathcal{L}}{\partial \dot{\tilde{\varphi}}} \right) = -K\tilde{\varphi} + \bar{u}_2 + Q_{\text{ext},2}, \quad (29)$$

which describes the relative motion of the two generalized inertias. We may rewrite (28) and (29) as

$$\Sigma_3 : \begin{bmatrix} m+b & b \\ b & b \end{bmatrix} \begin{bmatrix} \ddot{q}_u \\ \ddot{\tilde{\varphi}} \end{bmatrix} + \begin{bmatrix} 1 & 0 \\ 0 & k \end{bmatrix} \begin{bmatrix} g(q_u) \\ \tilde{\varphi} \end{bmatrix} = \mathcal{N}_2 (\bar{\mathbf{u}} + Q_{\text{ext}}). \quad (30)$$

This matrix form can also be obtained straightforwardly by applying the coordinate transformation (26) directly to dynamics equations (30). In Section 3, we use this shorter route to derive the concept for the multijoint case.

2.4 | Adopting energy-shaping for a series elastic joint

We are now in a position where we can comfortably adopt the energy-shaping technique. Since the noncollocated output now appears as quasi actuated, we can easily shift the equilibrium of the EL system and aim for a unique equilibrium at $q_u = q_d$. To this end, we span a virtual spring from the link to its desired position. In addition, we cancel the effect of the gravitational field such that the potential energy has a unique minimum at $(q_u, \tilde{\varphi}) = (q_d, 0)$. To render this equilibrium attractive, we attach a damper to each inertia. The resulting behavior is visualized in Figure 3(right). Canceling the effect of gravity and adding PD terms on the link side is precisely what we did in the rigid joint case. Thus, the control input as follows produces the desired behavior

$$\begin{bmatrix} \bar{u}_1 \\ \bar{u}_2 \end{bmatrix} = \begin{bmatrix} u_{PD} \\ -k_{v,2}\dot{\tilde{q}}_a \end{bmatrix}. \quad (31)$$

We observe that the first input equals the rigid joint control law (12). Obviously, we have to rewrite it in the link coordinate q_u . The second input is used to achieve full damping. This will be the general pattern throughout this article; see Figure 10(bottom) for a preview.

Why does the approach above work? Let's rederive (31), by directly applying the energy-shaping machinery, as introduced in Reference 2. To this end, we express our desired damping behavior in terms of a Rayleigh function

$$\mathcal{F}_d = \frac{1}{2} \begin{bmatrix} \dot{q}_u \\ \dot{\tilde{q}}_a \end{bmatrix}^T \mathcal{K}_v \begin{bmatrix} \dot{q}_u \\ \dot{\tilde{q}}_a \end{bmatrix}; = \frac{1}{2} \begin{bmatrix} \dot{q}_u \\ \dot{\tilde{\varphi}} \end{bmatrix}^T \mathbf{T}_2^{-T} \mathcal{K}_v \mathbf{T}_2^{-1} \begin{bmatrix} \dot{q}_u \\ \dot{\tilde{\varphi}} \end{bmatrix} \quad (32)$$

with the positive gain matrix $\mathcal{K}_v \triangleq \text{diag}(k_{v,1}, k_{v,2})$. It is important to note that $\mathcal{N}_2 = \mathbf{T}_2^{-T}$. The desired closed-loop potential energy is given by $\mathcal{V}_d = \mathcal{V}_e(\tilde{\varphi}) + \frac{1}{2}k_p\tilde{q}^2$. Our goal is to find a control input $\bar{\mathbf{u}}$ such that the closed-loop system is characterized by the EL parameters $\{\mathcal{T}(\dot{q}_u, \dot{\tilde{q}}_a), \mathcal{V}_d(q_u, \tilde{q}_a), \mathcal{F}_d(\dot{q}_u, \dot{\tilde{q}}_a)\}$. Considering (13) and the fact that \mathcal{N}_2 is invertible, applying²

$$\mathcal{N}_2 \bar{\mathbf{u}} = - \begin{bmatrix} \frac{\partial}{\partial q_u} \\ \frac{\partial}{\partial \tilde{\varphi}} \end{bmatrix} \mathcal{V}_e(q_u) - \begin{bmatrix} \frac{\partial}{\partial \dot{q}_u} \\ \frac{\partial}{\partial \dot{\tilde{\varphi}}} \end{bmatrix} \mathcal{F}_d(\dot{q}_u, \dot{\tilde{\varphi}}) \equiv \quad (33)$$

$$\bar{\mathbf{u}} = - \begin{bmatrix} \frac{\partial \mathcal{V}_e(q_u)}{\partial q_u} \\ 0 \end{bmatrix} - \mathcal{K}_v \mathbf{T}_2^{-1} \begin{bmatrix} \dot{q}_u \\ \dot{\tilde{\varphi}} \end{bmatrix} = \begin{bmatrix} u_{PD} \\ -k_{v,2}\dot{\tilde{q}}_a \end{bmatrix} \quad (34)$$

to (30) gives the desired result. The Hamiltonian of the closed-loop system is given by

$$\mathcal{H}_{cl} = \mathcal{T}(\dot{q}_u, \dot{q}_u + \dot{\tilde{\varphi}}) + \mathcal{V}_e(\tilde{\varphi}) + \frac{1}{2}k_p\tilde{q}^2, \quad (35)$$

where the latter two terms constitute the desired closed-loop potential energy.

2.5 | Simulation

This section analyzes the closed-loop behaviors of the rigid and flexible joint systems that are illustrated in Figures 2(right) and 3(right). That is, we consider system (9) under control of (12) and system (17) under control of (31). Both systems are initially at rest with the initial configuration $q_u = \varphi = 0$. The desired output position is $q_d = 0.1$ rad. The system and control parameters are summarized in Table 1.

The damping parameters are calculated as follows: $k_{v,1} = 2\xi\sqrt{m_k p}$ and $k_{v,2} = 2\xi\sqrt{b_s k}$, with b_s being the closed-loop motor inertia. The original and shaped motor inertias are related via the factor $\alpha \triangleq b_s/b$. We choose $\xi = 0.7$ in order to ensure a nice convergence behavior. Figures 5 and 6 show the step-responses for different motor inertia values that are due to motor inertia shaping, compare Table 1.

TABLE 1 System and control parameters

m	b	k	$k_{p,1}$	$k_{v,1}$	$k_{v,2}$	ξ	α
1	0.2	100	200	19.8	1.98	0.7	0.1
1	0.2	100	200	19.8	6.26	0.7	1
1	0.2	100	200	19.8	19.8	0.7	10

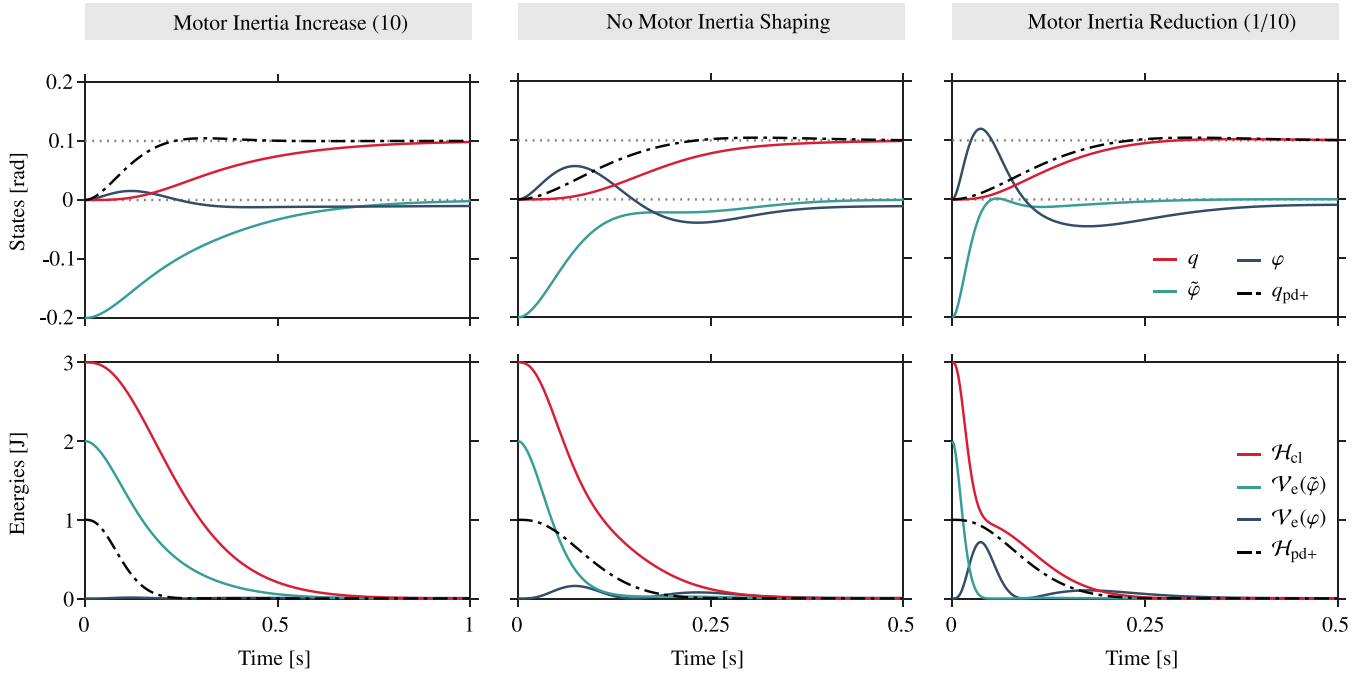


FIGURE 5 Step responses of the rigid and elastic joints in closed-loop with (12) and (31), as illustrated in Figures 2(right) and 3(right). The plots illustrate the effect of motor inertia shaping. As anticipated, the links converge to the desired position $q_d = 0.1$ rad and $\tilde{\varphi}$ converge to zero. The limit value of φ is given by the static equilibrium condition such that the spring torque balances the pull of gravity on the link. For decreasing values of the motor inertia, the elastic joint approaches the behavior of the rigid one (compare red versus black lines)

Remark 3. It makes no difference whether we shape the motor inertia first and then apply the input and state transformation on the shaped system, or, whether we apply the input and state transformation first and then shape the motor inertia utilizing the new motor-side input.

The state transformation allows for an elegant geometric interpretation. We can think of (19) as encoding a hyperplane embedded in three-dimensional Cartesian space. Each triplet $(\bar{u}_1/k, \varphi, \tilde{\varphi})$ that satisfies the state transformation (19) lies on that hyperplane. Hence, all solutions of (30) evolve on that plane. Projecting this hyperplane into the $\bar{u}_1/k, \varphi$ -plane allows the evolution of the deflection coordinates to be visualized in a 2D plot, see Figure 6. These isolines are straight since the curvature of the hyperplane is by definition zero at every point. Due to the scaling of the input axis, these isolines are parallel to the line $\varphi = \bar{u}_1/k$.

2.6 | Discussion

Note that the points discussed in the following generalize to the multijoint case which is introduced in Section 3. However, most aspects of the presented framework can be introduced more intuitively on the basis of a single joint since it provides us with a simple picture of the closed-loop dynamics.

A fundamental aspect of the proposed concept is that it enables damping and stiffness behaviors to be specified directly in terms of the noncollocated output (rigid coordinates). This allows for the output convergence behavior to be easily and physically intuitively adjusted. The tuning reduces to selecting the link-side stiffness and damping factors. The benefits of controller gains that come with a physical intuition cannot be overestimated for the commissioning and tuning stage of

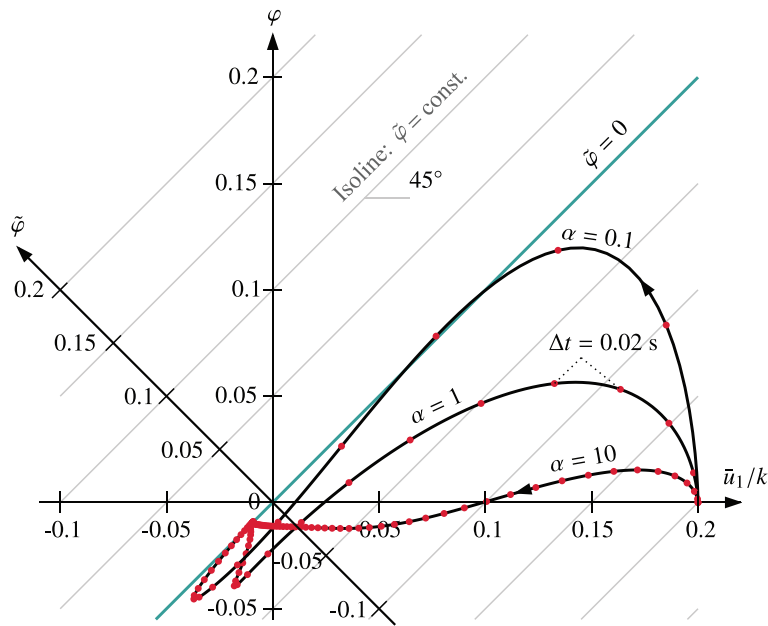


FIGURE 6 The coordinate transformation (19) can be interpreted as defining a hyperplane in 3D space. By scaling the desired input with the joint compliance, we can consider it as an additional deflection state. This allows us to visualize the state transformation as depicted. The basis vector spanning the virtual deflection space is rotated at an angle of 45 degrees relative to the basis vector of the physical deflection space. Since the origin of $(\tilde{\varphi}, \tilde{q})$ is globally asymptotically stable, the system tends to the one-dimensional subspace $\tilde{\varphi} = 0$, which is dual to tending to a zero torque error. Scaling the motor inertia allows us to adjust the rate of convergence in a physically intuitive way. The solutions for three different inertia shaping factors ($\alpha = 0.1, 1, 10$) are shown

a controller. This intuition is of particular importance when designing controllers for the safe interaction between robots and humans.

It is crucial to understand the effect of the motor inertias on the convergence behavior of the closed-loop system. During transients, physical intuition suggests that we can expect smaller spring deflections, $\tilde{\varphi}$, the smaller the motor inertia. Now considering $\tilde{\varphi}$'s dual nature to the joint torque error, compare (19), we conclude that the lower the motor inertia the closer the actual joint torque, $\tau(\varphi)$ approximates the desired joint torque \bar{u}_1 . This intuition is supported by the simulation results in Figure 5. Comparing Figures 2(right) and 3(right), we immediately see that by shaping the motor inertia to lower values, the faster the convergence of $\tilde{\varphi}$ to zero. Naturally, this behavior is also reflected in the decay rate of the potential energy $\mathcal{V}_e(\tilde{\varphi})$, (27). In other words, for small motor inertia values, the virtual input \bar{u}_1 dominates the elastic torque, $\tau(\tilde{\varphi})$, such that the dynamic behavior of the flexible joint approaches that of its corresponding rigid joint. Notice that not only the variations of q and q_{PD+} approach each other, but also the variations of the closed-loop energies of the rigid and elastic joints \mathcal{H}_{PD+} , (11), and \mathcal{H}_{cl} , (35). In practice, we obviously face limitations regarding to what degree the motor inertia can be lowered, since the control inputs must respect the limits imposed by the respective hardware.

Regarding the input transformation (24), it is interesting to consider the theoretical limit case $b \rightarrow 0$ and $k \rightarrow \infty$. In the first case, the control input u_2 approaches the rigid robot controller \bar{u}_1 . We observe the same tendency for the limit case $k \rightarrow \infty$. In conclusion, for the limit cases $k \rightarrow \infty$ and/or $b \rightarrow 0$, that would reduce the flexible joint model to the rigid one, the control input u_2 in (24) also reduces to the rigid robot equivalent. The closed-loop behavior in the “almost rigid” case is an important aspect. Clearly, we do want to avoid high-gain designs where the loop gains grow unbounded with increasing stiffness. See Reference 16 for a discussion of this aspect.

3 | A STRUCTURE PRESERVING INPUT AND STATE TRANSFORMATION

In this section, we extend the concept introduced in Section 2 to the multijoint case with nonlinear springs. This process can be shortened by introducing new deflection states directly, instead of introducing new motor states first. Figure 7 provides an overview of the single steps, which will be introduced in detail below. In Step 1 we perform a coordinate transformation.³⁷ Instead of considering the generalized coordinates (q_u, q_a) that represent the link and motor

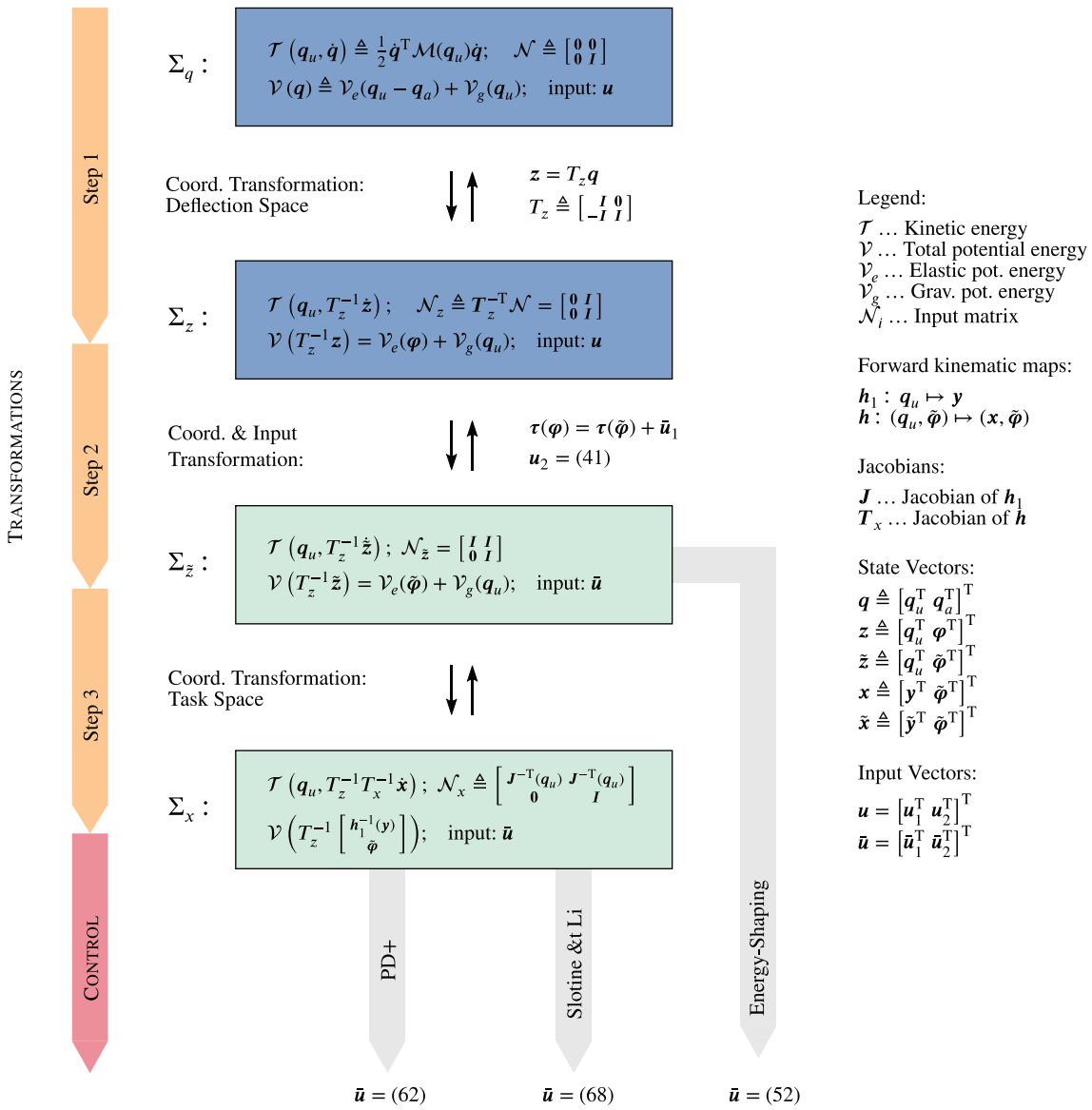


FIGURE 7 Overview of the general procedure of the proposed framework

coordinates respectively, we switch to a new set of generalized coordinates (q_u, φ) . We can think of this step as separating the generalized coordinates into rigid and elastic coordinates. In Step 2 we introduce a state and input transformation that allows us to treat the system as *quasi-fully actuated*. In Step 3 we perform another change of coordinates by expressing the rigid dynamics in terms of task (output) coordinates y .

3.1 | Step 1: Coordinate transformation into deflection space

Let us introduce the following coordinate transformation

$$\mathbf{z} = T_z q, \quad T_z \triangleq \begin{bmatrix} I & \mathbf{0} \\ -I & I \end{bmatrix}, \quad (36)$$

with the partitioning \mathbf{z} as $\mathbf{z} \triangleq [q_u^T \ \varphi^T]^T$. This step can be understood as a separation of the generalized coordinates into coordinates describing the rigid state, q_u , and the elastic state, φ . Applying this transformation to the system (4) gives

$$\Sigma_z : \mathcal{M}_z(q_u) \ddot{\mathbf{z}} + \mathcal{C}_z(q_u, \dot{q}_u) \dot{\mathbf{z}} + \boldsymbol{\psi}_z(\mathbf{z}) = \mathcal{N}_z \mathbf{u} + T_z^{-T} Q_{\text{ext}}, \quad (37)$$

where $\mathcal{M}_z(\mathbf{q}_u) \triangleq \mathbf{T}_z^{-T} \mathcal{M}(\mathbf{q}_u) \mathbf{T}_z^{-1}$ and $C_z(\mathbf{q}_u, \dot{\mathbf{q}}_u) \triangleq \mathbf{T}_z^{-T} C(\mathbf{q}_u, \dot{\mathbf{q}}_u) \mathbf{T}_z^{-1}$ denote the transformed inertia and Coriolis/centrifugal matrices, respectively, see Appendix A.3 for their full forms. Inspecting the transformed potential forces $\psi_z(\mathbf{z}) \triangleq \mathbf{T}_z^{-T} \psi(\mathbf{q}_u, \dot{\mathbf{q}}_u) = [\mathbf{g}^T(\mathbf{q}_u) \quad \boldsymbol{\tau}^T(\boldsymbol{\varphi})]^T$, we see a separation of the forces that are due to the rigid and elastic states. This separation will be key for later steps. The transformed inertia matrix \mathcal{M}_z now contains off-main-diagonal blocks. In conclusion, the rigid and elastic dynamics of Σ_z are solely coupled via the inertia matrix. The new input coupling matrix \mathcal{N}_z is given by $\mathcal{N}_z \triangleq \mathbf{T}_z^{-T} \mathcal{N} = \begin{bmatrix} \mathbf{0} & \mathbf{I} \\ \mathbf{0} & \mathbf{I} \end{bmatrix}$. The generalized external forces transform analogously to the input vector. Transforming the Hamiltonian function $\mathcal{H} : \mathbb{R}^{4n} \rightarrow \mathbb{R}$, (2), under (36) reveals the separation of the rigid body and elastic potential energies

$$\mathcal{H}(\mathbf{T}_z^{-1}\dot{\mathbf{z}}, \mathbf{T}_z^{-1}\mathbf{z}) = \frac{1}{2}\dot{\mathbf{z}}^T \mathcal{M}_z \dot{\mathbf{z}} + \mathcal{V}(\mathbf{T}_z^{-1}\mathbf{z}) = \frac{1}{2}\dot{\mathbf{z}}^T \mathcal{M}_z \dot{\mathbf{z}} + \mathcal{V}_g(\mathbf{q}_u) + \mathcal{V}_e(\boldsymbol{\varphi}). \quad (38)$$

3.2 | Step 2: State and input transformation

Inspired by Section 2, let us introduce new deflection states that are in a dual relationship with the joint force error through the diffeomorphism

$$\boldsymbol{\tau}(\boldsymbol{\varphi}) = \boldsymbol{\tau}(\tilde{\boldsymbol{\varphi}}) + \bar{\mathbf{u}}_1. \quad (39)$$

Compared to (19), we now have vector-valued functions on both sides that are no longer linear functions in the general case. Vector $\bar{\mathbf{u}}_1$ will be our link-side input vector of the quasi-fully actuated form. In the case of a robot with no elastic couplings, see for example, Figure 10(right), we observe that the state transformation (39) is composed of n independent scalar relations

$$\tau_i(\boldsymbol{\varphi}_i) = \tau_i(\tilde{\boldsymbol{\varphi}}_i) + \bar{u}_{1,i}, \quad i = 1, 2, \dots, n. \quad (40)$$

Each of the new deflection states $\tilde{\boldsymbol{\varphi}}_i$ depends solely on the i th deflection $\boldsymbol{\varphi}_i$ and the i th input $\bar{u}_{1,i}$. Analogous to (19), (40) establishes a duality between the joint force error $\boldsymbol{\tau}(\tilde{\boldsymbol{\varphi}})$ and the new deflection state $\tilde{\boldsymbol{\varphi}}$. Figure 8 visualizes this dualism by showing an exemplary relation of the form (40). Geometrically, we can think of these relations as each defining a hypersurface embedded in a 3-dimensional Euclidean space as visualized in Figure 9(left). Each triplet $(\boldsymbol{\varphi}_i, \tilde{\boldsymbol{\varphi}}_i, \bar{u}_{1,i})$ satisfying (39) defines a point on the corresponding hypersurface. As the system evolves with time, each point will trace out a curve on its associated surface. Figure 9(right) shows two exemplary trajectories for a system that is subject to a

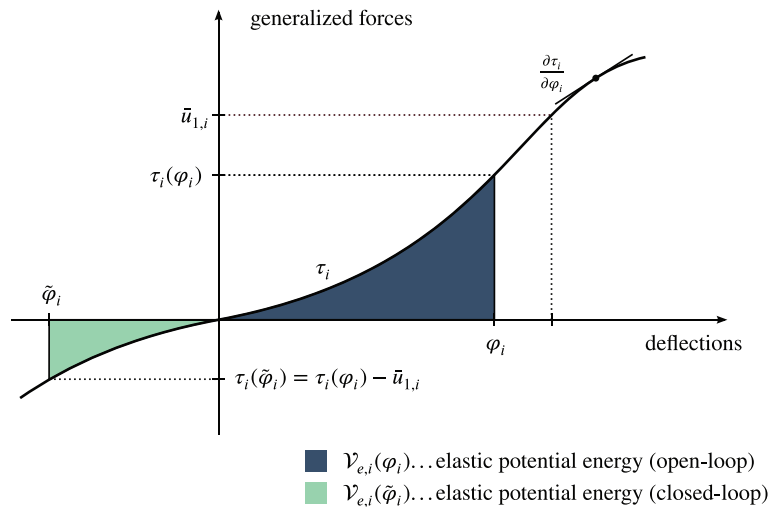


FIGURE 8 State transformation for nonlinear springs: deflection states. The blue and green areas under the torque profile curve represent the elastic potential energy of the open and closed-loop systems, respectively

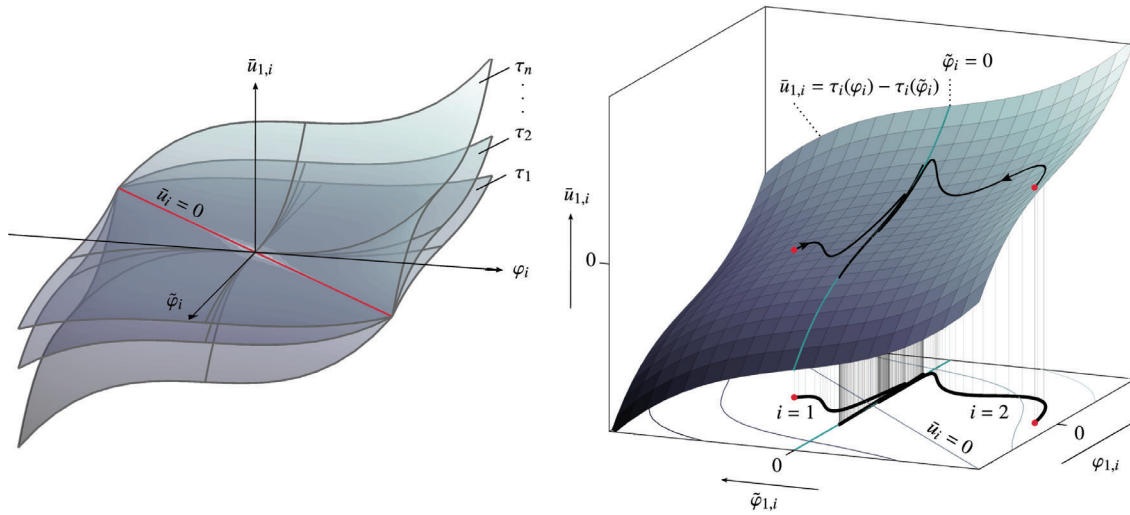


FIGURE 9 (Left) Each of the transforming equations (40) defines hypersurface whose shape is uniquely determined by the joint torque functions τ_i . In general, these hypersurfaces may intersect each other. However, they always intersect at least once along the line defined by $\varphi_i = \tilde{\varphi}_i$. (Right) The deflection state of each joint is represented by a point on a hypersurface. Its contour lines are projected on the bottom. In contrast to joints with linear springs, these are no longer straight lines, compare Figure 6. In order to draw the time trajectories of two configuration points on one hypersurface we assumed w.l.o.g that $\tau_1 = \tau_2$. The trajectories shown are exemplary motions of a two-link planar manipulator under adopted PD+ control, see Section 5.2

stabilizing feedback control law $\bar{\mathbf{u}}$. For simplicity, we assumed that the torque characteristics of both joints are equal, that is, $\tau_1 = \tau_2$. It is crucial to note that both deflection vectors are related by a diffeomorphism. This follows directly from Assumption 1 on the elastic potential \mathcal{V}_e . We are now in the position to derive an input transformation Γ of the form

$$\mathbf{u}_2 = \mathbf{A}(\varphi, \bar{\mathbf{u}}_1)\bar{\mathbf{u}}_2 + \Gamma(\mathbf{z}, \dot{\mathbf{z}}, \bar{\mathbf{u}}_1, \dot{\bar{\mathbf{u}}}_1, \ddot{\bar{\mathbf{u}}}_1), \quad (41)$$

such that applying the state and input transformations (39) and (41) to system (37) yields the desired quasi-fully actuated form

$$\Sigma_{\tilde{\mathbf{z}}} : \mathcal{M}_{\mathbf{z}}(\mathbf{q}_u)\ddot{\mathbf{z}} + \mathcal{C}_{\mathbf{z}}(\mathbf{q}_u, \dot{\mathbf{q}}_u)\dot{\mathbf{z}} + \boldsymbol{\psi}_{\mathbf{z}}(\tilde{\mathbf{z}}) = \mathcal{N}_{\tilde{\mathbf{z}}}(\bar{\mathbf{u}} + \mathcal{Q}_{\text{ext}}^{\star}), \quad (42)$$

where $\tilde{\mathbf{z}} = [\mathbf{q}_u^T, \tilde{\varphi}^T]^T$. Matrix \mathbf{A} is diagonal, positive definite and contains the ratios of the stiffness values expressed in the respective deflection spaces

$$\mathbf{A}(\tilde{\varphi}, \varphi) = \tau_{\varphi}^{-1}(\varphi)\tau_{\tilde{\varphi}}(\tilde{\varphi}). \quad (43)$$

A detailed derivation of (41) is presented in Appendix A. We observe that for uncoupled systems the input transformation (41) is composed of n independent scalar equations of the form $\Gamma_i(\varphi_i, \dot{\varphi}_i, \bar{u}_{1,i}, \dot{\bar{u}}_{1,i}, \ddot{\bar{u}}_{1,i})$, where $\Gamma_i : \mathbb{R}^5 \rightarrow \mathbb{R}$ for $i = 1, \dots, n$. Comparing (42) and (37), we observe that the structure of the LHS is fully preserved. Thus, considering $\tilde{\mathbf{z}}, \dot{\tilde{\mathbf{z}}}$ as new system states, it is immediately clear that $\Sigma_{\tilde{\mathbf{z}}}$ is characterized by the *same* EL parameters as the original system $\Sigma_{\mathbf{z}}$, and thus, by the same Hamiltonian function \mathcal{H} . The only structural difference can be found on the RHS with the new input matrix $\mathcal{N}_{\tilde{\mathbf{z}}} = \begin{bmatrix} \mathbf{I} & \mathbf{I} \\ \mathbf{0} & \mathbf{I} \end{bmatrix}$, which is now of full rank, and the new input vector $\bar{\mathbf{u}} = [\bar{\mathbf{u}}_1^T \quad \bar{\mathbf{u}}_2^T]^T$. Further, in the case of nonlinear springs, the external forces acting on the motor inertias are scaled. We have that $\mathcal{Q}_{\text{ext}}^{\star} \triangleq \left[\mathcal{Q}_{\text{ext},1}^T (\mathbf{A}^{-1} \mathcal{Q}_{\text{ext},2})^T \right]^T$. In summary, the EL parameters of system $\Sigma_{\tilde{\mathbf{z}}}$ are given by $\{\mathcal{T}(\mathbf{q}_u, \mathbf{T}_z^{-1}\dot{\mathbf{z}}), \mathcal{V}(\mathbf{T}_z^{-1}\tilde{\mathbf{z}}), 0, \mathcal{N}_{\tilde{\mathbf{z}}}, \mathcal{Q}_{\text{ext}}^{\star}\}$. Figure 10(left) provides an overview. At this point it might be tempting to consider system (42) as fully actuated. However, some weak limitations exist on which feedback signals can be contained in $\bar{\mathbf{u}}_1$ as we discuss in the remark below. Furthermore, the desired torques $\bar{\mathbf{u}}_1$ must be at least twice differentiable with respect to time. This constraint is imposed by the intrinsic physics of the systems. For a compliant torque controlled system, it is physically impossible to cause a jump in the joint torque, and thus on the link-side torque $\bar{\mathbf{u}}_1$. Due to these weak constraints, we call system (42) *quasi-fully actuated*.

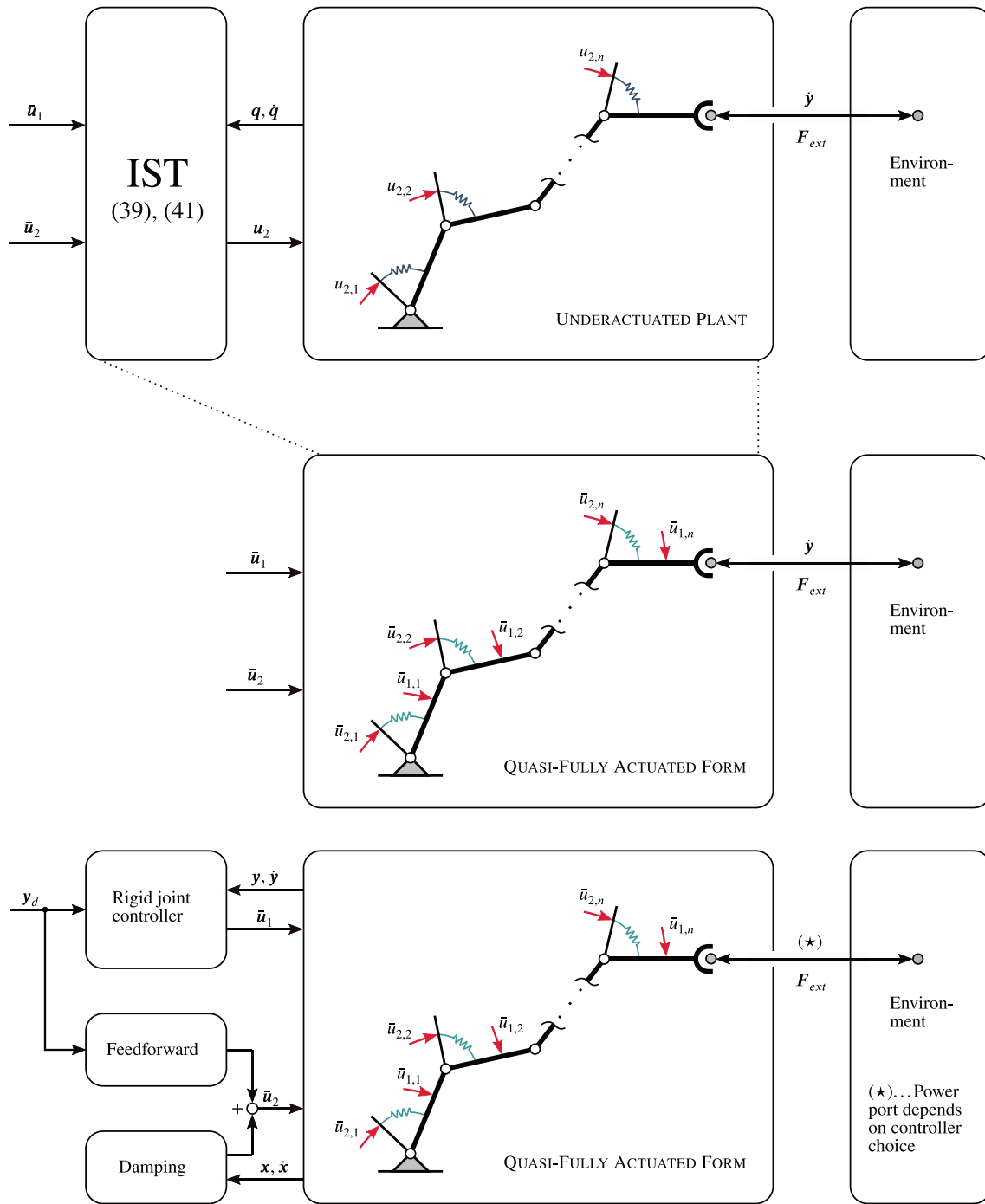


FIGURE 10 (Top) General framework: under the proposed input and state transformation (IST) the robot can be treated as quasi-fully actuated. (Bottom) Closed-loop: the quasi-fully actuated form enables a straightforward adoption of rigid joint controllers

Suppose that the control signal \bar{u}_1 contains feedback of the rigid states q_u, \dot{q}_u . Then, the implementation of (41) requires knowledge of \dot{q}_u and $q_u^{(3)}$. It is worth remarking that these signals can be computed without numerical differentiation. Using the model equations (4), the final control input can always be expressed as full state feedback in terms of z, \dot{z} . This is a fundamental property of the Spong model,¹⁷ which is lost in the complete model.³⁸ At the DLR, we utilize this method for implementing our state-of-the-art controllers,^{30,31,39} see Reference 40 for details.

Notice that the state and input transforming equations (39) and (41) that produce the QFA form by itself do not alter the dynamics of the plant. These transforming equations “merely” allow us to rewrite the system dynamics of an underactuated ASRs in a more tractable form by making the transformed dynamics behave as if fully actuated. In

other words, (37) and (42) are equivalent models representing the dynamics of an ASR. From (39) and (41) it is clear that $\bar{\mathbf{u}} = \mathbf{0} \Rightarrow \boldsymbol{\varphi} \equiv \tilde{\boldsymbol{\varphi}} \Rightarrow \mathbf{A} \equiv \mathbf{I} \Rightarrow \mathbf{u}_2 = \mathbf{0}$. Thus, only at the moment of implementing a particular controller via the virtual inputs, we alter the system dynamics. Loosely speaking, the system shaping scales with the magnitude of the rigid input vector. Compared to two-stage schemes,¹³ (41) does not represent an inner control loop that “preshapes” the dynamics.

For the special case of linear springs such that $\tau(\boldsymbol{\varphi}) = \mathbf{K}\boldsymbol{\varphi}$, where \mathbf{K} is a positive definite matrix containing the joint stiffness coefficients, the input transformation (41) simplifies to

$$\mathbf{u}_2 = \bar{\mathbf{u}}_2 + \bar{\mathbf{u}}_1 + \mathbf{B}\mathbf{K}^{-1}\ddot{\bar{\mathbf{u}}}_1. \quad (44)$$

Again, for systems with no elastic couplings the input transformation (44) constitutes n independent scalar equations of the form $u_{2,i} = \bar{u}_{2,i} + \bar{u}_{1,i} + B_{ii}K_{ii}^{-1}\ddot{\bar{u}}_{1,i}$. The state transformation (39) simplifies to

$$\boldsymbol{\varphi} = \tilde{\boldsymbol{\varphi}} + \mathbf{K}^{-1}\bar{\mathbf{u}}_1, \quad (45)$$

which are n independent scalar equations of the form $\varphi_i = \tilde{\varphi}_i + \bar{u}_{1,i}/K_{ii}$, $i = 1, 2, \dots, n$. Each of these linear relations is of the form as visualized in Figure 4. Thus, we have the same geometrical interpretation of the new deflection states as in the single joint case.

3.3 | Some energy considerations

In Step 2 in Section 3.2, we introduced a set of state and input transforming equations, (39), and (41) to transform (37) into its QFA form (42). Note that this transformation does not represent a point transformation⁴¹ or canonical transformation.³⁷ As a consequence, the principle of *scalar invariance*⁴² does not hold, and, in general, the Hamiltonians associated with the systems Σ_z and $\Sigma_{\tilde{z}}$ do not evaluate to the same values for $\bar{\mathbf{u}}_1 \neq \mathbf{0}$. We can, however, quantify the difference in energies between the open-loop and closed-loop systems

$$\begin{aligned} \Delta\mathcal{H} &\triangleq \mathcal{H}(\mathbf{T}_z^{-1}\mathbf{z}, \mathbf{T}_z^{-1}\dot{\mathbf{z}}) - \mathcal{H}(\mathbf{T}_{\tilde{z}}^{-1}\tilde{\mathbf{z}}, \mathbf{T}_{\tilde{z}}^{-1}\dot{\tilde{\mathbf{z}}}) \\ &= \mathcal{V}_e(\boldsymbol{\varphi}) + \frac{1}{2}(\dot{\mathbf{q}} + \dot{\boldsymbol{\varphi}})^T \mathbf{B} (\dot{\mathbf{q}} + \dot{\boldsymbol{\varphi}}) - \left[\mathcal{V}_e(\tilde{\boldsymbol{\varphi}}) + \frac{1}{2}(\dot{\mathbf{q}} + \dot{\tilde{\boldsymbol{\varphi}}})^T \mathbf{B} (\dot{\mathbf{q}} + \dot{\tilde{\boldsymbol{\varphi}}}) \right]. \end{aligned} \quad (46)$$

In case the closed-loop motor inertia was shaped, one has to adapt the motor inertia matrix in the associated kinetic energy term accordingly. Using the diffeomorphism (36) allows us to rewrite the energy difference $\Delta\mathcal{H}$ as a function of only the physical states $\mathbf{q}, \boldsymbol{\varphi}$ and the control input $\bar{\mathbf{u}}_1$ —or vice-versa—as a function of the virtual states $\mathbf{q}, \tilde{\boldsymbol{\varphi}}$ and the control input $\bar{\mathbf{u}}_1$. In other words, knowing the energy of the transformed QFA system, we can always compute the energy of the associated real system via (46). Note that $\bar{\mathbf{u}}_1 \equiv \mathbf{0}$ implies $\boldsymbol{\varphi} \equiv \tilde{\boldsymbol{\varphi}}$, and, thus $\Delta\mathcal{H} \equiv \mathbf{0}$. In future works, it seems worth investigating the possibility of using (46) to quantify the system shaping imposed through a particular control law choice for $\bar{\mathbf{u}}_1$.

It is worth remarking that planning for ASRs is usually done in terms of the outputs, that is, the link coordinates \mathbf{q}_u . Considering the fact that ASRs satisfying Assumption 1 are differentially flat implies that any given $\mathbf{q}_u(t)$ trajectory uniquely determines the necessary variation of actuator torques $\mathbf{u}(t)$, and the corresponding motor trajectories, \mathbf{q}_a . However, knowing the time evolution of the link and motor trajectories, $\mathbf{q}_u(t)$ and $\mathbf{q}_a(t)$, implies knowing the time evolution of the total energy of the real system. In summary, defining a link trajectory \mathbf{q}_u uniquely defines the total energy variation, $\mathcal{H}(\mathbf{q}(t), \dot{\mathbf{q}}(t))$, of the real system. In the end, it does not matter if we plan the output trajectory on the real or quasi-fully actuated system, since at all times the links evolve equally.

4 | ADOPTING THE ENERGY-SHAPING CONCEPT

Continuing with the quasi-fully actuated form (42), compare Figure 10(top), we demonstrate how the global asymptotic stabilization problem, $\tilde{\mathbf{q}}_u \rightarrow \mathbf{0}$ for $t \rightarrow \infty$, where $\tilde{\mathbf{q}}_u \triangleq \mathbf{q}_u - \mathbf{q}_d$ denotes the output error, may be solved by adopting the classical energy-shaping and damping injection technique introduced in Reference 2. Our goal is to shape the potential

energy of system $\Sigma_{\tilde{\mathbf{z}}}$ such that the potential energy of the closed-loop system is radially unbounded and has a unique global minimum at the target point $\tilde{\mathbf{z}}_d = [\mathbf{q}_d^T \quad \mathbf{0}]^T$. Knowing that the Hamiltonian associated with $\Sigma_{\tilde{\mathbf{z}}}$ is

$$\mathcal{H}(\mathbf{T}_{\tilde{\mathbf{z}}}^{-1}\tilde{\mathbf{z}}, \mathbf{T}_{\tilde{\mathbf{z}}}^{-1}\dot{\tilde{\mathbf{z}}}) = \mathcal{T}(\mathbf{q}_u, \mathbf{T}_{\tilde{\mathbf{z}}}^{-1}\dot{\tilde{\mathbf{z}}}) + \mathcal{V}(\mathbf{T}_{\tilde{\mathbf{z}}}^{-1}\tilde{\mathbf{z}}) = \frac{1}{2}\dot{\tilde{\mathbf{z}}}^T \mathcal{M}_{\tilde{\mathbf{z}}}(\mathbf{q}_u)\dot{\tilde{\mathbf{z}}} + \mathcal{V}_e(\tilde{\boldsymbol{\varphi}}) + \mathcal{V}_g(\mathbf{q}_u), \quad (47)$$

we conclude from Assumption 1 that the elastic potential energy is radially unbounded with respect to $\tilde{\boldsymbol{\varphi}}$ and has a unique minimum at $\tilde{\boldsymbol{\varphi}} = \mathbf{0}$. Thus, we can minimize the shaping of the system dynamics by shaping only the potential energy connected with the rigid coordinates. To this end, let the desired closed-loop potential energy be of the form

$$\mathcal{V}_d(\tilde{\mathbf{z}}) \triangleq \mathcal{V}(\mathbf{T}_{\tilde{\mathbf{z}}}^{-1}\tilde{\mathbf{z}}) + \mathcal{V}_c(\mathbf{q}_u), \quad (48)$$

where \mathcal{V}_c is the potential function of the controller. Applying the controller

$$\bar{\mathbf{u}} = -\mathcal{N}_{\tilde{\mathbf{z}}}^{-1} \left(\frac{\partial \mathcal{V}_c}{\partial \tilde{\mathbf{z}}}(\mathbf{q}_u) \right)^T = - \begin{bmatrix} \left(\frac{\partial \mathcal{V}_c}{\partial \mathbf{q}_u}(\mathbf{q}_u) \right)^T \\ \mathbf{0} \end{bmatrix} \quad (49)$$

to (42), the potential function of system $\Sigma_{\tilde{\mathbf{z}}}$ takes on the desired one, $\mathcal{V}_d(\tilde{\mathbf{z}})$, see Reference 2 for details. The Hamiltonian of the controlled system is thus given by $\mathcal{H}_d(\tilde{\mathbf{z}}, \dot{\tilde{\mathbf{z}}}) = \mathcal{T}(\mathbf{q}_u, \dot{\tilde{\mathbf{z}}}) + \mathcal{V}_d(\tilde{\mathbf{z}})$.

We present two basic options for $\mathcal{V}_d(\tilde{\mathbf{z}})$ to achieve global asymptotic stability. First, we can cancel the gravitational potential $\mathcal{V}_g(\mathbf{q}_u)$ and replace it with a radially unbounded potential function in \mathbf{q}_u that has a unique minimum at \mathbf{q}_d . Second, we can dominate the effect of the gravitational potential.^{2,43} It is widely believed that dominating instead of canceling nonlinear terms enhances robustness of the system vis-a-vis parametric uncertainties.^{33,44} Let us continue with two simple examples for each case. Regarding the first option, we may choose

$$\mathcal{V}_d(\tilde{\mathbf{z}}) = \mathcal{V}_e(\tilde{\boldsymbol{\varphi}}) + \frac{1}{2}\tilde{\mathbf{q}}_u^T \mathbf{K}_q \tilde{\mathbf{q}}_u, \quad (50)$$

where \mathbf{K}_q is a positive definite and symmetric matrix. Regarding the second option, we may choose

$$\mathcal{V}_d(\tilde{\mathbf{z}}) = \mathcal{V}(\tilde{\mathbf{z}}) - \mathcal{V}(\tilde{\mathbf{z}}_d) - \frac{\partial \mathcal{V}}{\partial \tilde{\mathbf{z}}}(\tilde{\mathbf{z}}_d)(\tilde{\mathbf{z}} - \tilde{\mathbf{z}}_d) + \frac{1}{2}\tilde{\mathbf{q}}_u^T \mathbf{K}_q \tilde{\mathbf{q}}_u, \quad (51)$$

where \mathbf{K}_q can be chosen such that \mathcal{V}_d becomes a strictly convex function with a global minimum $\mathcal{V}_d(\tilde{\mathbf{z}}) = 0$ at $\tilde{\mathbf{z}} = \mathbf{0}$, as demonstrated in Reference 2. It is straightforward to see that the resulting controller potential is again a function of the rigid coordinates only. To achieve full damping, we select an appropriate Rayleigh damping function $\mathcal{F}(\tilde{\mathbf{q}}_u, \dot{\tilde{\boldsymbol{\varphi}}})$ and extend (49) to

$$\bar{\mathbf{u}} = - \begin{bmatrix} \left(\frac{\partial \mathcal{V}_c}{\partial \mathbf{q}_u}(\mathbf{q}_u) \right)^T \\ \mathbf{0} \end{bmatrix} - \mathcal{N}_{\tilde{\mathbf{z}}}^{-1} \frac{\partial \mathcal{F}}{\partial \dot{\tilde{\mathbf{z}}}}(\dot{\tilde{\mathbf{z}}}). \quad (52)$$

See Reference 33 for details on energy shaping via Rayleigh functions. For example, the Rayleigh damping function

$$\mathcal{F}(\dot{\tilde{\mathbf{z}}}) = \frac{1}{2}\dot{\tilde{\mathbf{z}}}^T \mathbf{T}_{\tilde{\mathbf{z}}}^{-T} \mathbf{D} \mathbf{T}_{\tilde{\mathbf{z}}}^{-1} \dot{\tilde{\mathbf{z}}}, \quad \text{with } \mathbf{D} \triangleq \begin{bmatrix} \mathbf{D}_1 & \mathbf{0} \\ \mathbf{0} & \mathbf{D}_2 \end{bmatrix}, \quad (53)$$

with positive definite symmetric matrices $\mathbf{D}_1, \mathbf{D}_2 \in \mathbb{R}^{n \times n}$ achieves a fully-damped system. It is easy to see that \mathcal{F} qualifies as a Rayleigh function (e.g., by invoking Sylvester's law of inertia). Considering that $\mathcal{N}_{\tilde{\mathbf{z}}} = \mathbf{T}_{\tilde{\mathbf{z}}}^{-T}$, we can get for control input (52)

$$\bar{\mathbf{u}} = - \begin{bmatrix} \left(\frac{\partial \mathcal{V}_c}{\partial \mathbf{q}_u}(\mathbf{q}_u) \right)^T \\ \mathbf{0} \end{bmatrix} - \mathbf{D} \mathbf{T}_{\tilde{\mathbf{z}}}^{-1} \dot{\tilde{\mathbf{z}}}. \quad (54)$$

Knowing that $\mathbf{T}_z^{-1}\dot{\tilde{\mathbf{z}}} = [\dot{\mathbf{q}}_u^T \quad \dot{\tilde{\mathbf{q}}}_a]$, it is clear that \mathcal{F} ensures that $\bar{\mathbf{u}}_1$ is independent of the deflection velocities $\dot{\tilde{\mathbf{q}}}$. Hence, our assumptions on the state transformation (39) are satisfied. We can interpret (53) as injecting damping proportional to the rigid body and virtual motor velocities $\dot{\tilde{\mathbf{q}}}_a$, (A9). We can now invoke Proposition 3 in the Appendix to conclude global asymptotic stability.

5 | ADOPTING TASK-SPACE CONTROLLERS

In this section, we demonstrate how to solve the task-space tracking problem by adopting tracking controllers that have been originally designed for fully actuated systems. As it turns out, it also allows us to adopt the stability analysis machinery developed for these controllers with some adjustments. We showcase this on the basis of two popular passivity-based controllers. Specifically, we choose the PD+ controller and the Slotine and Li controller since both adhere closely to the idea of minimal system shaping. The PD+ controller can be interpreted as impedance control with feedforward terms, since it allows to specify a compliant behavior of the robot's TCP with respect to a reference trajectory.

5.1 | Step 3: Coordinate transformation into task space

As we aim to analyze and control the dynamic behavior of the robot's end-effector in task space, it is rewarding to formulate the dynamics of $\Sigma_{\tilde{\mathbf{z}}}$, (42), in terms of task coordinates. Considering (6), and applying the change of coordinates

$$\mathbf{x} = \mathbf{h}(\mathbf{q}_u, \tilde{\boldsymbol{\varphi}}) = \begin{bmatrix} \mathbf{h}_1(\mathbf{q}_u) \\ \tilde{\boldsymbol{\varphi}} \end{bmatrix}; \quad \dot{\mathbf{x}} = \mathbf{T}_x(\mathbf{q}_u)\dot{\tilde{\mathbf{z}}}; \quad \mathbf{T}_x(\mathbf{q}_u) \triangleq \begin{bmatrix} \mathbf{J}(\mathbf{q}_u) & \mathbf{0} \\ \mathbf{0} & \mathbf{I} \end{bmatrix} \in \mathbb{R}^{n \times n}, \quad (55)$$

to (42) gives

$$\Sigma_x : \mathcal{M}_x(\mathbf{y})\ddot{\mathbf{x}} + \mathcal{C}_x(\mathbf{y}, \dot{\mathbf{y}})\dot{\mathbf{x}} + \boldsymbol{\psi}_x(\mathbf{x}) = \mathcal{N}_x(\bar{\mathbf{u}} + \mathcal{Q}_{\text{ext}}^{\star}), \quad (56)$$

with the transformed system matrices $\mathcal{M}_x(\mathbf{y}) = \mathbf{T}_x^{-T}\mathcal{M}_z(\mathbf{q}_u)\mathbf{T}_x^{-1}$ and $\mathcal{C}_x(\mathbf{y}, \dot{\mathbf{y}}) = \mathbf{T}_x^{-T}\mathcal{M}_z\dot{\mathbf{T}}_x^{-1} + \mathbf{T}_x^{-T}\mathcal{C}_z(\mathbf{q}_u, \dot{\mathbf{q}}_u)\mathbf{T}_x^{-1}$. See Reference 3 for details on how these relations can be established. Crucially, the separation of the potential forces into rigid body and elastic forces is preserved. Applying the transformation rule for covariant vectors, we get

$$\boldsymbol{\psi}_x(\mathbf{x}) \triangleq \mathbf{T}_x^{-T}\boldsymbol{\psi}(\mathbf{h}^{-1}(\mathbf{x})) = \begin{bmatrix} \mathbf{J}^{-T}(\mathbf{h}_1^{-1}(\mathbf{y}))\mathbf{g}(\mathbf{h}_1^{-1}(\mathbf{y})) \\ \boldsymbol{\tau}(\tilde{\boldsymbol{\varphi}}) \end{bmatrix}.$$

The transformed Hamiltonian is $\mathcal{H}(\mathbf{h}^{-1}(\mathbf{x}), \mathbf{T}_x^{-1}(\mathbf{q}_u)\dot{\mathbf{x}})$. Generalized forces \mathcal{Q} transform to $\mathbf{T}_x^{-T}(\mathbf{q}_u)\mathcal{Q}$. Thus, for the new control input matrix \mathcal{N}_x we have[‡]

$$\mathcal{N}_x \triangleq \mathbf{T}_x^{-T}(\mathbf{q}_u)\mathcal{N}_{\tilde{\mathbf{z}}} \quad (57)$$

which is again of full rank. See Reference 3 for an introduction regarding system transformations into task space. Let $\mathbf{y}_d \in \mathbb{C}^4$ be the desired trajectory of the end-effector in task-space. We define the tracking error as $\tilde{\mathbf{x}} \triangleq \mathbf{x} - \mathbf{x}_d$ with $\mathbf{x}_d(t) \triangleq [\mathbf{y}_d(t)^T \quad \mathbf{0}]^T$. Note that this choice implies that the desired deflection error is zero.

Remark 4. The actual implementation of the task-space controllers in Sections 5.2 and 5.3 does not require the calculation of the inverse transformation.

5.2 | Adopting PD+ control

Motivated by the work,⁴⁵ we aim for a PD+ like error dynamics[§]

$$\mathcal{M}_x(\mathbf{q}_u)\ddot{\tilde{\mathbf{x}}} + (\mathcal{C}_x(\mathbf{q}_u, \dot{\mathbf{q}}_u) + \mathcal{K}_v(\mathbf{q}_u))\dot{\tilde{\mathbf{x}}} + \mathcal{K}_p\tilde{\mathbf{x}} + \boldsymbol{\psi}_e(\tilde{\boldsymbol{\varphi}}) = \mathcal{N}_x\mathcal{Q}_{\text{ext}}^{\star}, \quad (58)$$

with $\psi_e(\tilde{\varphi}) \triangleq [\mathbf{0} \quad \tau^T(\tilde{\varphi})]^T$ and gain matrices $\mathcal{K}_p \triangleq \text{blockdiag}(\mathcal{K}_{p,1}, \mathbf{0})$ and

$$\mathcal{K}_v(\mathbf{q}_u) \triangleq \underbrace{\mathbf{T}_x^{-T} \mathbf{T}_z^{-T} \mathbf{T}_x^T}_{\mathcal{N}_x(\mathbf{q}_u)} \begin{bmatrix} \mathcal{K}_{v,1} & \mathbf{0} \\ \mathbf{0} & \mathcal{K}_{v,2} \end{bmatrix} \mathbf{T}_x \mathbf{T}_z^{-1} \mathbf{T}_x^{-1}, \quad (59)$$

where $\mathcal{K}_{v,i} = \mathcal{K}_{v,i}^T > 0$, $i = (1, 2)$, and $\mathcal{K}_{p,1} = \mathcal{K}_{p,1}^T > 0$. Considering the storage function

$$\mathcal{H}_{pd+}(t, \tilde{\mathbf{x}}, \dot{\tilde{\mathbf{x}}}) = \frac{1}{2} \dot{\tilde{\mathbf{x}}}^T \mathcal{M}_x(t, \tilde{\mathbf{y}}) \dot{\tilde{\mathbf{x}}} + \mathcal{V}_e(\tilde{\varphi}) + \frac{1}{2} \tilde{\mathbf{x}}^T \mathcal{K}_p \tilde{\mathbf{x}}, \quad (60)$$

it is easy to see that system (58) defines an output strictly passive operator $\Sigma_{pd+} : Q_{ext}^* \mapsto \dot{\tilde{\mathbf{x}}}$ system (58) defines an output strictly passive operator $\Sigma_{pd+} : Q_{ext}^* \mapsto \tilde{\mathbf{x}}$ which can be demonstrated with the following. Differentiating \mathcal{H}_{pd+} with respect to time along the trajectories of (58) yields

$$\dot{\mathcal{H}}_{pd+} = -\dot{\tilde{\mathbf{x}}}^T \mathcal{K}_v \dot{\tilde{\mathbf{x}}} + \dot{\tilde{\mathbf{x}}}^T Q_{ext}^*. \quad (61)$$

Introducing virtual motor velocities $\dot{\tilde{\mathbf{q}}}_a = \dot{\tilde{\varphi}} + \mathbf{J}^{-1}(\mathbf{q}_u) \dot{\mathbf{y}}$, and $\dot{\mathbf{q}}_{a,d} \triangleq \mathbf{J}^{-1} \dot{\mathbf{y}}_d$, $\dot{\tilde{\mathbf{q}}}_a \triangleq \dot{\tilde{\mathbf{q}}}_a - \dot{\mathbf{q}}_{a,d}$, $\tilde{\mathbf{y}} \triangleq \mathbf{y} - \mathbf{y}_d$, it is straightforward to show that the desired dynamics (58) is obtained by applying the following control input to (56)

$$\bar{\mathbf{u}} = \begin{bmatrix} \mathbf{u}_r \\ \mathbf{u}_d \end{bmatrix} = \begin{bmatrix} \mathbf{J}^T (\mathbf{M}_y \dot{\mathbf{y}}_d + \mathbf{C}_y \ddot{\mathbf{y}}_d - \mathcal{K}_{v,1} \dot{\tilde{\mathbf{y}}} - \mathcal{K}_{p,1} \tilde{\mathbf{y}}) + \mathbf{g}(\mathbf{q}_u) \\ \mathbf{B} \dot{\mathbf{q}}_{a,d} - \mathcal{K}_{v,2} \dot{\tilde{\mathbf{q}}}_a \end{bmatrix}. \quad (62)$$

The inertia and coriolis/centrifugal matrices \mathbf{M}_y and \mathbf{C}_y are reported in the Appendix A.3. Control input \mathbf{u}_r equals the PD+ control signal for the rigid-joint robot case.⁵ Control input \mathbf{u}_d has some clear physical meaning. Vector $\dot{\mathbf{q}}_{a,d}$ represents the desired task accelerations expressed in joint space. Thus, the feedforward term in \mathbf{u}_d ensures that the motor inertias accelerate synchronously with link inertias. The second term adds damping to eliminate any velocity error. We now summarize the main result of this section. A proof is provided in Section 6.

Proposition 1 (Tracking with PD+ control). *In absence of external forces Q_{ext} , the nonlinear static state feedback control (62) solves the global tracking problem in task space. The equilibrium point $[\tilde{\mathbf{x}}^T \quad \dot{\tilde{\mathbf{x}}}^T]^T = \mathbf{0}$ of the closed-loop system (58) is globally uniformly asymptotically stable. A Lyapunov function to prove this is given by (60). Further, system (58) defines an OSP map $\mathcal{N}_x Q_{ext}^* \mapsto \dot{\tilde{\mathbf{x}}}$.*

Remark 5. Analyzing (61), we identify an interconnection port $\dot{\mathbf{y}}^T \mathbf{J}^{-T}(\mathbf{q}_u) Q_{ext,1} = \dot{\mathbf{y}}^T F_{ext}$ that exchanges energy between the robot and its environment. In practice, many situations may arise where passivity with respect to the power port $(\dot{\mathbf{y}}, F_{ext})$ would be of importance. More specifically, situations exist where the environment or the interacting object move synchronously to the TCP reference trajectory. Possible scenarios would be object manipulation on a conveyor belt or a task that requires interaction with a moving human subject. In that case, the controlled robot would passively interact with the object. Note that for the regulation case passivity with respect to the physically more intuitive power port $(\dot{\mathbf{y}}, F_{ext})$ is given.

5.3 | Adopting the Slotine and Li controller

Motivated by Slotine and Li,⁴⁶ we aim for an error dynamics of the form

$$\mathcal{M}_x(t, \tilde{\mathbf{y}}) \dot{\mathbf{s}} + (\mathcal{C}_x(t, \tilde{\mathbf{y}}, \dot{\tilde{\mathbf{y}}}) + \mathcal{K}_v) \mathbf{s} + \psi_e(\tilde{\varphi}) = \Psi + \mathcal{N}_x Q_{ext}^*, \quad (63)$$

with diagonal⁴⁷ positive definite matrices $\mathcal{K}_v = \text{diag}(\mathcal{K}_{v,1}, \mathcal{K}_{v,2})$, $\Lambda = \text{diag}(\Lambda_1, \Lambda_2)$ of appropriate dimensions, and error signal

$$\mathbf{s} \triangleq \begin{bmatrix} \mathbf{s}_y^T & \mathbf{s}_\varphi^T \end{bmatrix}^T = \dot{\tilde{\mathbf{x}}} + \Lambda \tilde{\mathbf{x}}. \quad (64)$$

The key observation here is that (63) defines an output strictly operator $\Sigma : (\Psi + \mathcal{N}_x Q_{\text{ext}}^*) \mapsto s^{48}$ with storage function

$$\mathcal{H}_s(t, \tilde{\phi}, s) \triangleq \frac{1}{2} s^T \mathcal{M}_x s + \mathcal{V}_e(\tilde{\phi}). \quad (65)$$

Calculating its time derivative along the solutions of (63) and using the skew-symmetry property (3) yields[#]

$$\dot{\mathcal{H}}_s(t, \tilde{\phi}, s) = -s^T \mathcal{K}_v s - \tilde{\phi}^T \Lambda_2 \tau(\tilde{\phi}) + s^T (\Psi + \mathcal{N}_x Q_{\text{ext}}^*). \quad (66)$$

Consequently, for $\Psi = Q_{\text{ext}} = \mathbf{0}$, we have $s \in \mathcal{L}_2$, compare Reference 33. Straight forward calculations show that (42) is equivalent to (63) with

$$\Psi = \mathcal{N}_x \bar{u} - (\mathcal{M}_x \ddot{x}_r + C_x \dot{x}_r + \psi_g(q_u) - \mathcal{K}_v s), \quad (67)$$

where the reference velocity $\dot{x}_r \triangleq \dot{x}_d - \Lambda \tilde{x}$ is partitioned as $\dot{x}_r^T \triangleq [\dot{y}_r^T \ \dot{\tilde{\phi}}_r^T]$, and $\psi_g(q_u) \triangleq [(J^{-T}(q_u) g(q_u))^T \ \mathbf{0}]^T$ represents the gravity forces expressed in task-space. The control input \bar{u} that sets $\Psi \equiv \mathbf{0}$ is obtained in an obvious manner

$$\bar{u} = \begin{bmatrix} u_r \\ u_d \end{bmatrix} = \begin{bmatrix} J^T (\mathbf{M}_y \ddot{y}_r + \mathbf{C}_y \dot{y}_r - \mathcal{K}_{v,1} s_y) + g(q_u) \\ B \ddot{q}_{a,r} - \mathcal{K}_{v,2} (J^{-1} s_y + s_\phi) \end{bmatrix}, \quad (68)$$

where $\dot{q}_{a,r} \triangleq \dot{\tilde{\phi}}_r + J^{-1}(q_u) \dot{y}_r$ can be interpreted as “motor reference velocity” vector. Notice the structural analogy to the coordinate transformation (36) stating $\dot{q}_a = \dot{\phi} + \dot{q}_u = \dot{\phi} + J^{-1}(q_u) \dot{y}$. Input u_r is the Slotine and Li controller for the rigid robot case.⁶ Input u_d contains feed-forward and damping terms ensuring asymptotic converges of the elastic coordinates $\tilde{\phi}$ to the origin. The main results of this section are summarized in the following proposition. A proof is presented in the Section 6.

Proposition 2 (Tracking with Slotine and Li controller). *The nonlinear static state feedback control (68) solves the global tracking problem in task space. The origin of the resulting closed-loop system (63) is globally asymptotically stable. Further, system (63) defines an OSP map $\mathcal{N}_x Q_{\text{ext}}^* \mapsto s$.*

6 | STABILITY ANALYSIS

This section reports proofs for Propositions 1 and 2.

6.1 | Proof of Proposition 1 (via Matrosov's Theorem)

In this section, we proof Proposition 1. In order to show uniform asymptotic stability of (58), we adopt the core technique that has been applied in the original work of the PD+ controller.⁵ We use storage function (60) as Lyapunov function and invoke Matrosov's Theorem. In Reference 30, we showed how Matrosov's theorem can be applied to solve the global asymptotic joint-space tracking problem for ASRs. Here, we highlight only the key steps and adjustments required compared to Reference 30. The challenge lies in verifying that Condition (4) of Matrosov's theorem is satisfied. Thus, Condition (4) is at the center of focus in the proof below.

Proof. We consider $\mathcal{H}_{\text{pd+}} : ([0, \infty] \times \Omega) \rightarrow \mathbb{R}$ as an energy based, time-variant, Lyapunov function candidate. For now, set Ω can be chosen arbitrarily large. We summarize our states into a new state vector $e \triangleq [\tilde{x}^T \ \dot{\tilde{x}}^T]^T$. Evaluating the time derivative of $\mathcal{H}_{\text{pd+}}$ along the solutions of (58), for $Q_{\text{ext}} = \mathbf{0}$, gives

$$\dot{\mathcal{H}}_{\text{pd+}}(t, \tilde{x}, \dot{\tilde{x}}) = -\frac{1}{2} \dot{\tilde{x}}^T \mathcal{K}_v \dot{\tilde{x}} \quad (69)$$

which is a negative semidefinite function of the states. Thus $\mathcal{H}_{\text{pd+}}$ qualifies as Lyapunov function. It is straightforward to see that Condition (1) of Matrosov's Theorem is satisfied. Next, we show that $\mathcal{H}_{\text{pd+}}(t, \tilde{x}, \dot{\tilde{x}})$ is lower and upper bounded by functions of class \mathcal{K} . Let us consider the state-dependent bounding functions

$$\alpha(\tilde{\mathbf{x}}) = \frac{1}{2} \left(\inf_{t \in I, \mathbf{e} \in \Omega} \lambda(\mathcal{M}_x(t, \tilde{\mathbf{x}})) \|\dot{\tilde{\mathbf{x}}}\|^2 + \inf \lambda(\mathbf{K}_x) \|\tilde{\mathbf{y}}\|^2 \right) + \mathcal{V}_e(\tilde{\boldsymbol{\varphi}}),$$

$$\beta(\tilde{\mathbf{x}}) = \frac{1}{2} \left(\sup_{t \in I, \mathbf{e} \in \Omega} \lambda(\mathcal{M}_x(t, \tilde{\mathbf{x}})) \|\dot{\tilde{\mathbf{x}}}\|^2 + \sup \lambda(\mathbf{K}_x) \|\tilde{\mathbf{y}}\|^2 \right) + \mathcal{V}_e(\tilde{\boldsymbol{\varphi}}),$$

where $\lambda(\cdot)$ denotes the eigenvalue of (\cdot) . By invoking¹⁵ lemma 4.3, we can conclude the existence of class \mathcal{K} functions a and b such that $a(\|\tilde{\mathbf{x}}\|) \leq \alpha(\tilde{\mathbf{x}})$ and $b(\|\tilde{\mathbf{x}}\|) \geq \beta(\tilde{\mathbf{x}})$. In fact, a and b will be of class \mathcal{K}_∞ , since α and β are radially unbounded. This allows us to conclude uniform stability of the origin of Σ_{pd+} and that Condition (1) of Matrosov's Theorem is satisfied.

The central idea of Matrosov's Theorem relies on the appealing usage of a bounded auxiliary function that ensures that the system cannot get stuck in the problematic set, $E = \{\mathbf{e} \in \Omega : \dot{\tilde{\mathbf{x}}} = \mathbf{0}\}$, where the time-derivative of the Lyapunov function is zero. We choose this auxiliary function $W : [0, \infty) \times \Omega \rightarrow \mathbb{R}$ as

$$W(t, \mathbf{e}) \triangleq \dot{\mathcal{H}}_{pd+}(t, \mathbf{e}), \quad (70)$$

and restrict Ω to be an arbitrarily large, but bounded set. Exploiting the fact that the origin is stable, one can show that Condition (3) is satisfied. One may apply the same line of arguments as introduced in Reference 30. Computing the time derivative of W along the solutions of (58) and evaluating \dot{W} on the critical set E yields

$$\dot{W}(t, \mathbf{e}) = -2 \begin{bmatrix} \tilde{\mathbf{y}} \\ \tau(\tilde{\boldsymbol{\varphi}}) \end{bmatrix}^T \mathbf{P}(t, \tilde{\mathbf{y}}) \begin{bmatrix} \tilde{\mathbf{y}} \\ \tau(\tilde{\boldsymbol{\varphi}}) \end{bmatrix}, \quad (71)$$

where

$$\mathbf{P}(t, \tilde{\mathbf{y}}) \triangleq \text{blockdiag}(\mathbf{K}_x^T, \mathbf{I}) \mathcal{M}_x^{-T} \mathcal{K}_v \mathcal{M}_x^{-1} \text{blockdiag}(\mathbf{K}_x, \mathbf{I}). \quad (72)$$

The properties of \mathcal{M}_x and the assumptions on \mathcal{K}_v and \mathbf{K}_x imply that \mathbf{P} is a positive matrix which is state- and explicitly time-dependent. This allows us to establish the inequality $|\dot{W}(t, \mathbf{e})| \geq W^*(\mathbf{e})$, $\forall \mathbf{e} \in E$, where $W^*(\mathbf{e}) \triangleq \inf_{t \in I, \mathbf{e} \in \Omega} \lambda(\mathbf{P}(t, \tilde{\mathbf{y}})) \left\| \begin{bmatrix} \tilde{\mathbf{y}} & \tau(\tilde{\boldsymbol{\varphi}}) \end{bmatrix} \right\|^2$ is a time-invariant and positive definite function of the states. By invoking⁴⁹ lemma 4.3, we can conclude the existence of class \mathcal{K}_∞ function γ such that $W^*(\mathbf{e}) \geq \gamma(\|\mathbf{e}\|)$. We conclude that

$$|\dot{W}(\mathbf{e})| \geq \gamma(\|\mathbf{e}\|) \quad \forall \mathbf{e} \in E \quad \text{and} \quad t \in [0, \infty]. \quad (73)$$

Invoking Lemma 1, that was proposed in Reference 5, (73) ensures that the critical Condition (4) of Matrosov's Theorem is satisfied.⁵⁰ Fulfillment of Condition (5) can be shown in straightforward manner, see also Reference 30 for details. This ends the proof. ■

Roughly speaking, we showed that near E and away from the origin, the rate of change of a second bounded auxiliary function is of constant sign and bounded away from zero. Thus, the state cannot remain near E , and away from the origin, without driving W beyond its bounds. Hence, the only point in E to which the system state can converge is the origin.

6.2 | Proof of Proposition 2 (via strict Lyapunov function)

The closed-loop dynamics (63)–(64) we study closely resembles that of the rigid robot case.⁵¹ The difference are the generalized elastic forces (represented by the last term on the LHS of (63)). Due to the conservative nature of the generalized elastic forces we can adapt the techniques proposed in Reference 47. A similar approach is applied in Reference 33 which consider linear elastic elements and joint-space tracking only, however.

Proof. Let us consider the Lyapunov function candidate

$$\mathcal{V} = \frac{1}{2} \mathbf{s}^T \mathcal{M}_x(t, \tilde{\mathbf{y}}) \mathbf{s} + \tilde{\mathbf{y}}^T \Lambda_1 \mathcal{K}_{v,2} \tilde{\mathbf{y}} + \mathcal{V}_e(\tilde{\boldsymbol{\varphi}}). \quad (74)$$

We extended the storage function (65) with an explicit quadratic term in $\tilde{\mathbf{y}}$ that is positive definite. This ensures that (74) qualifies as Lyapunov function candidate since it is a global positive definite function.⁵⁰ Recall that \mathbf{K}_x and Λ_1 are both diagonal. The difference in the Lyapunov function candidate for the rigid robot case⁴⁷ is the addition of the elastic potential energy $\mathcal{V}_e(\tilde{\boldsymbol{\varphi}})$. A similar approach was chosen in Evaluating the time derivative of (74) along the solution of (63) yields

$$\dot{\mathcal{V}} = -\mathbf{s}^T \mathcal{K}_v \mathbf{s} - \tilde{\boldsymbol{\varphi}}^T \Lambda_2 \boldsymbol{\tau}(\tilde{\boldsymbol{\varphi}}) + 2\tilde{\mathbf{y}}^T \Lambda_1 \mathcal{K}_{v,2} \dot{\mathbf{y}}, \quad (75)$$

where we have used the skew-symmetry property (3). With the partitioning $\mathbf{s} \triangleq [\mathbf{s}_y^T \quad \mathbf{s}_\varphi^T]^T$ and using the relations summarized in Appendix A.3.1 and the definition of \mathcal{K}_v , (59), we may rewrite the first term in (75) as

$$\begin{aligned} \mathbf{s}^T \mathcal{K}_v \mathbf{s} &= (\mathbf{T}_z^{-1} \mathbf{T}_x^{-1} \mathbf{s})^T \mathbf{T}_x^T \begin{bmatrix} \mathcal{K}_{v,1} & \mathbf{0} \\ \mathbf{0} & \mathcal{K}_{v,2} \end{bmatrix} \mathbf{T}_x (\mathbf{T}_z^{-1} \mathbf{T}_x^{-1} \mathbf{s}) \\ &= \begin{bmatrix} \mathbf{J}^{-1} \mathbf{s}_y \\ \mathbf{J}^{-1} \mathbf{s}_y + \mathbf{s}_\varphi \end{bmatrix}^T \begin{bmatrix} \mathbf{J}^T \mathcal{K}_{v,1} \mathbf{J} & \mathbf{0} \\ \mathbf{0} & \mathcal{K}_{v,2} \end{bmatrix} \begin{bmatrix} \mathbf{J}^{-1} \mathbf{s}_y \\ \mathbf{J}^{-1} \mathbf{s}_y + \mathbf{s}_\varphi \end{bmatrix} \\ &= \dot{\tilde{\mathbf{y}}}^T \mathcal{K}_{v,1} \dot{\tilde{\mathbf{y}}} + \tilde{\mathbf{y}}^T \Lambda_1^T \mathcal{K}_{v,1} \Lambda_1 \tilde{\mathbf{y}} + 2\tilde{\mathbf{y}}^T \Lambda_1 \mathcal{K}_{v,2} \dot{\tilde{\mathbf{y}}} + (\mathbf{J}^{-1} \mathbf{s}_y + \mathbf{s}_\varphi)^T \mathcal{K}_{v,2} (\mathbf{J}^{-1} \mathbf{s}_y + \mathbf{s}_\varphi), \end{aligned} \quad (76)$$

where the first equality follows directly from the definition of the gain matrix (59). Next, we substituted the definition of the error signal (64) and regrouped some terms. The last equality follows from the diagonal nature of the gain matrices Λ_1 and $\mathcal{K}_{v,1}$. Replacing (76) in (75) yields

$$\dot{\mathcal{V}} = -\dot{\tilde{\mathbf{y}}}^T \mathcal{K}_{v,1} \dot{\tilde{\mathbf{y}}} - \tilde{\mathbf{y}}^T \Lambda_1^T \mathcal{K}_{v,1} \Lambda_1 \tilde{\mathbf{y}} - \tilde{\boldsymbol{\varphi}}^T \Lambda_2 \boldsymbol{\tau}(\tilde{\boldsymbol{\varphi}}) - (\mathbf{J}^{-1} \mathbf{s}_y + \mathbf{s}_\varphi)^T \mathcal{K}_{v,2} (\mathbf{J}^{-1} \mathbf{s}_y + \mathbf{s}_\varphi). \quad (77)$$

It follows from (77) and Assumption 1 that $\dot{\mathcal{V}}$ is a negative semidefinite function which is only equal to zero if, and only if, all states $(\tilde{\mathbf{x}}, \dot{\tilde{\mathbf{x}}})$ are zero. We complete the proof by invoking Lyapunov's direct method. Since all states $(\tilde{\mathbf{x}}, \dot{\tilde{\mathbf{x}}})$ are bounded for bounded initial conditions, we can conclude boundedness of the original deflection states $(\boldsymbol{\varphi}, \dot{\boldsymbol{\varphi}})$ which follows directly from the state transformation (39). ■

Remark 6. In (77) we can identify an interesting term that has no direct connection to the rigid-joint case. The third in (77) represents the energy-loss rate due to the torque error. Thus, by adjusting gain Λ_1 , we can adjust the rate of convergence of the torque error.

7 | SIMULATION RESULTS

In this section, we present computer simulations to verify the stability and performance characteristics inferred from the theoretical developments. We consider a 2R manipulator composed of two identical links that is carrying a load, as indicated in Figure 11(left). At each joint, a serial elastic actuator (SEA) is mounted. We start with introducing the simulation setup.

7.1 | Simulation setup

The torque characteristics of the series elastic actuators (SEAs) are modeled by a third-order polynomial

$$\tau_i(\boldsymbol{\varphi}) \triangleq a_{i,1} \boldsymbol{\varphi} + a_{i,2} \boldsymbol{\varphi}^3, \quad (78)$$

with coefficients $a_{i,1} = 200 \text{ N rad}^{-1}$, $a_{i,2} = 2000 \text{ N rad}^{-3}$. The parameters are chosen such that the resulting torque characteristics resemble roughly the one of the floating spring joint (FSJ) featured in the DLR hand arm system introduced in Reference 11. The mechanical properties of the robot are summarized in Table 2. The motor inertias are denoted by b and the length of each link is given by l . At each link a mass m is located at the center. In addition, an external load of mass m_{load} is located at the tip (TCP) of the distal link. We assumed a maximal motor torque of $u_i \leq 60 \text{ N m}$ for each actuator. This is approximately three times the maximum torque required for the nominal motion. Considering this constraint, we manually tuned the controllers. The gain matrices are chosen with $\mathcal{K}_p = \text{diag}(500, 500)$, $\mathcal{K}_{v,1} = \text{diag}(47.5, 37.5)$, $\mathcal{K}_{v,2} =$

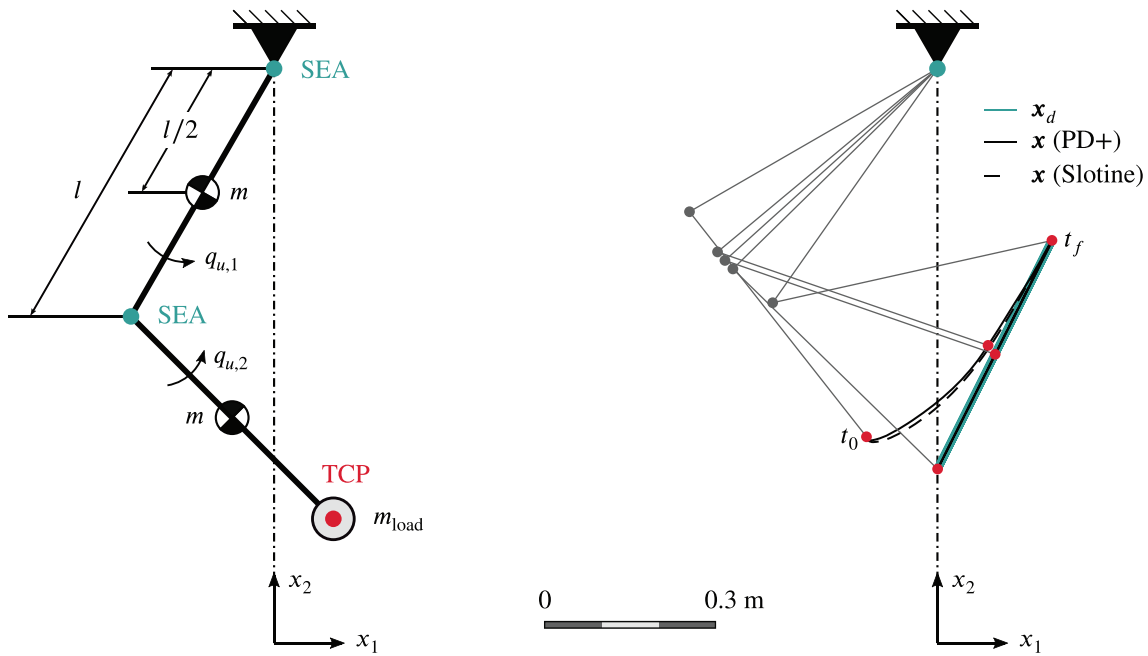


FIGURE 11 (Left) Robot model under consideration for simulation. A compliant two-link planar robot with nonlinear joint springs carrying a load. (Right) The desired trajectory (blue), and the actual TCP trajectories for PD+ (solid) and Slotine & Li (dashed) controllers are shown. Starting with the initial configuration, the robot poses are shown in 0.25 s intervals (PD+)

TABLE 2 Parameters of the planar two-link compliant robot

m [kg]	m_{load} [kg]	b [kg m^{-2}]	l [m]
1	1	0.2	0.5

$\text{diag}(5, 5)$ for the PD+ controller and with $\mathcal{K}_{v,1} = \text{diag}(15, 15)$, $\mathcal{K}_{v,2} = \text{diag}(10, 10)$, $\Lambda_1 = \text{diag}(15, 15)$ and $\Lambda_2 = \text{diag}(10, 10)$ for the Slotine and Li controller. All gain values are given in SI units.

7.2 | Simulation results

This section demonstrates the stability and performance characteristics of the PD+ and Slotine & Li adoptions presented in Section 5.2 and 5.3, and concludes with a comparison. In both experiments, the objective is to move the load on a task-space trajectory, as shown in Figure 11(right). The robot TCP is required to move back and forth on a straight line starting at $(x, y) = (0, 0.3)$ m and ending at $(x, y) = (0.2, 0.7)$ m with a frequency of once per second. The parameterization of the desired trajectory \mathbf{x}_d is

$$x_{d,i} = A_i \sin(\omega t + p_i) + c_i, \quad (79)$$

with $\omega = 2\pi$ rads $^{-1}$, $A_1 = 0.1$ m, $A_2 = 0.2$ m, $p_1 = p_2 = 3\pi/2$, $c_1 = 0.1$ m and $c_2 = 0.5$ m. The results for the PD+ (Slotine and Li) controller are plotted in solid (dashed) lines. In each run, the robot is initialized (at time $t_0 = 0$) with the configuration $(q_{u,1}, q_{u,2}) = (q_{a,1}, q_{a,2}) = (-\pi/3, 6\pi/11)$ rad which is visualized in Figure 11(right). We note that the robot system starts with zero joint deflections ($\boldsymbol{\varphi} = \mathbf{0}$) and thus zero spring torques (no static equilibrium configuration).

The actual and virtual joint deflections are plotted in Figure 12E, which shows the system's evolution on the hyperplane denoted by (39) projected into the $(\varphi_i, \tilde{\varphi}_i)$ -plane, compare Figure 9(right). The contour lines of the link-side input $\bar{u}_{1,i}$ as a function of the joint deflections φ_i and $\tilde{\varphi}_i$ are shown in gray. The initial points are marked with an “x”. The initial conditions of the virtual closed-loop system are dictated by (39). Since we have $\bar{u}_1 \neq \mathbf{0}$ in each case, compare Figure 12D, the quasi-fully actuated (closed-loop) systems are initialized with nonzero joint deflections ($\tilde{\varphi} \neq \mathbf{0}$), compare Figure 12E. Interestingly, since the PD+ and Slotine and Li controller initiate with different input values \bar{u}_1 we have differing initial

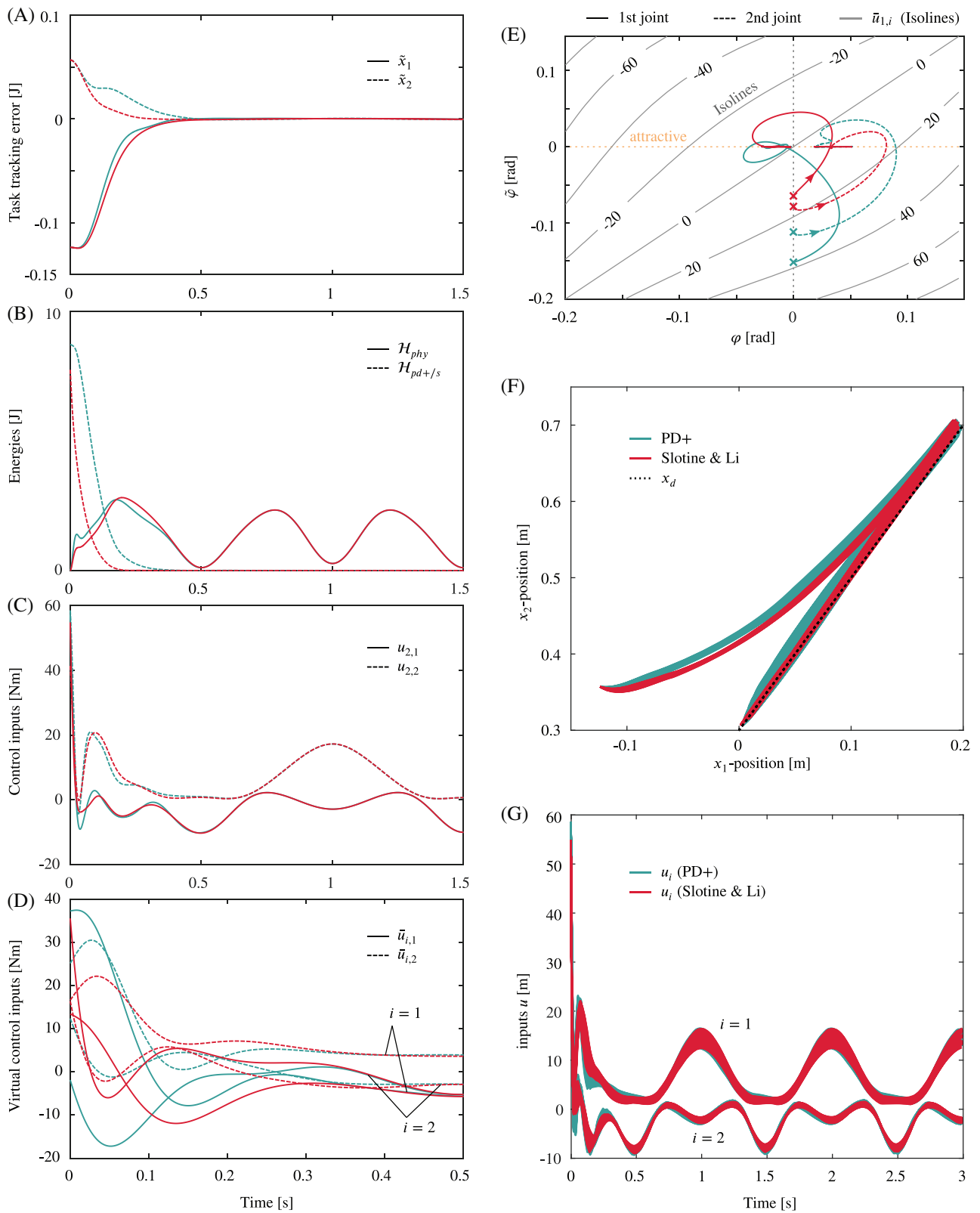


FIGURE 12 (A–D) Adopted PD+ (blue lines) and Slotine & Li (red lines) control. (A) TCP tracking error (cf. Figure 11(right)). (B) Physical energies H_{phy} and storage functions (60) and (65), respectively, (C) Control inputs acting on the actual robot. (D) Inputs acting on the quasi-fully actuated system (note the scaling of the time axis for better readability), compare Figure 10(right) for input definitions. (E) Actual and virtual joint deflections for PD+ (solid) and Slotine and Li (dashed) controllers. The contour lines of the link-side input $\bar{u}_{1,i}$ as a function of the joint deflections φ_i and $\dot{\varphi}_i$, defined via the state transformation (39), are shown in black. (F–G) Monte Carlo simulation: (F) tracking performance, (G) control inputs

deflection errors $\tilde{\varphi}$. As anticipated from our stability analysis the subset $\{\tilde{\varphi}_i \in \mathbb{R} \mid \tilde{\varphi}_i = 0\}$ is attractive. As such, for $t \rightarrow \infty$, the point defined by the triplet $(\varphi_i, \tilde{\varphi}_i, \bar{u}_i)$ slides along a one-dimensional submanifold on the hyperplane defined by (39). We observe that the Slotine and Li controller starts with slightly lower deflection errors and shows a smoother convergence behavior, which is a general trend, we observed in simulations. Figure 12A–D shows the tracking errors and control input as well as the system energies for the two controllers. As anticipated from the stability analysis in Section 6, the control errors converge to zero, see Figure 12A.

Both controllers inject similar levels of energy into the system and show comparable convergence rates. The total physical energy of the robot is denoted by \mathcal{H}_{phy} , see Figure 12B. The closed-loop storage functions (60) and (65) are denoted by \mathcal{H}_{pd+} and \mathcal{H}_s , respectively. Interestingly, albeit the control input \mathbf{u}_2 varying similarly with time, the (virtual) inputs $\bar{\mathbf{u}}_1$ and $\bar{\mathbf{u}}_2$ to the quasi-fully actuated systems show quite a different behavior during convergence, compare Figure 12C,D.

In order to analyze the robustness of the adopted controllers against model parameter uncertainties, we performed a Monte Carlo simulation. The load mass m_{load} , the motor inertia values, and the torque profile parameters $\alpha_{i,1}$ and $\alpha_{i,2}$ of the robot were randomly sampled in an interval of $\pm 20\%$ around the nominal values given above. We repeated the random sampling 100 times and analyzed the control performance of the PD+ and Slotine and Li controllers each time. The robot was commanded to follow the same desired trajectory as above, see (79), and starts from the same initial configuration. All results are combined in Figure 12F,G showing: (F) the tracking performance, and (G) the control inputs. The Slotine and Li controllers appears to have a slightly better tracking performance. However, on average, both controllers result in a root mean square error for $\dot{\mathbf{x}}$ of 0.03 m. In both cases, the control input magnitudes deviate only slightly from the nominal ones.

It is very difficult to derive a definite conclusion about performance differences of different controllers. The original rigid robot controllers are both PBC designs and derived from fundamental energy-based considerations, compare References 4 and 6 yielding designs with enhanced robustness properties that do not need cancelation of nonlinearities. The results demonstrate that rigid robot controllers that are expected to show a similar performance on rigid robots also show a similar performance when adopted through the presented concept of quasi-full actuation. From the practical point of view it seems worth mentioning that the PD+ controller allows for nondiagonal gain matrices, and thus, permitting modal decomposition based damping designs that adapt the gain layout online to the varying robot inertia and joint stiffnesses, see Reference 30 for details. In both cases, no lower or upper bounds on the controller gains are imposed. In particular, the link-side stiffness that characterizes the interaction of the robot with the environment can be increased above the intrinsic stiffness of the robot.

7.3 | Discussion

This work focuses on the theoretical aspects of the presented framework and how it simplifies the control design for underactuated compliant robots. The practical applicability of the framework has been confirmed in numerous experiments on the anthropomorphic DLR robot *David* with variable stiffness actuators (VSA). In References 28 and 30 we introduced a globally asymptotically stable joint-space motion tracking approach. Motion tracking and impact experiments can be found here:

- <https://youtu.be/PATvv47QfQs>

The robustness of this approach is highlighted in a demonstration where *David* drills into a block of concrete. This task requires both precise positioning of the tool center point and vibration damping, see:

- <https://youtu.be/JVdufPRK4NI>

In Reference 31, we present an asymptotically stable Cartesian impedance regulation controller with remarkable stiffness and damping range. Experiments showing task-space human-robot interaction and disturbance rejection behavior are shown here:

- <https://youtu.be/sbhiNNIxMNQ>

All these passivity-based concepts can be unified and elegantly expressed in the presented framework. Importantly, through the presented adoption of for example, the PD+ and Slotine and Li controllers, we were able achieve

asymptotically stable tasks-space motion tracking. To the best of our knowledge, these are the first PBC approaches that enable task-space motion tracking for compliant robots with nonlinear spring characteristics. The PD+ adoption can be considered a tasks-space impedance control with tracking behavior. It allows to specify a compliant behavior of the robot TCP with respect to a reference trajectory thereby enabling a compliant and passive interaction with moving objects.

8 | CONCLUSION

In this article, we have addressed the problem of controlling compliant manipulators with nonlinear stiffness characteristics. We introduced an Euler–Lagrange structure preserving state and input transformation that enables treating these underactuated systems as *quasi-fully* actuated. As a consequence, the framework allows a direct transfer of classical rigid robot control methods. Compared to existing solutions, the proposed scheme is not based on an inner feedback loop that cancels nonlinearities. Neither does it require any singular perturbation assumptions. In addition, the fact that the *quasi-fully* actuated form exhibits the same Euler–Lagrange structure as the original system facilitates physically motivated design approaches. This has several theoretical and practical advantages. The transfer of physically motivated control schemes potentially yields designs with enhanced robustness properties that do not require cancellation of nonlinearities. The benefits of a closed-loop dynamics that boasts a physically intuitive behavior can hardly be overestimated. In particular, by endowing the engineer with an intuitive feeling for the controller gains, it simplifies and quickens controller tuning during the commissioning stage. In conformity with this control philosophy, we showcased the adaption of popular rigid robot controllers: (1) energy-shaping concept, (2) PD+ controller, (3) Slotine and Li controller. The latter two resulted in passivity-based control designs that solved the task-space tracking problem while simultaneously achieving a desired compliance behavior of the robot's TCP with respect to a reference trajectory.

In future works, we will address adoption of whole-body control schemes and adaptive schemes that can cope with uncertainty in the robot parameters. Extensive experimental results on robotic systems that were presented in our previous works demonstrate the practical viability and robustness of the presented framework. We believe that our framework presents an important step toward unifying the control design for rigid and ASRs.

CONFLICT OF INTEREST

The authors declared that they have no conflict of interest.

DATA AVAILABILITY STATEMENT

Data sharing is not applicable to this article as no datasets were generated or analyzed during the current study.

ENDNOTES

*A change of configuration coordinates q of the form $(q, t) \rightarrow (q', t)$ that preserve the structure of Lagrange's equations.

[†]In this work we only consider the case of fully-damped closed-loop systems, which is a sufficient but not necessary condition. For certain inertia matrices partial damping is sufficient.³⁴

[‡]For convenience and better readability, we occasionally use the link coordinates instead of the task coordinates as function arguments, and sometimes drop the arguments altogether to shorten the expressions. Notice that we may switch back and forth between both sets of coordinates since they are related via diffeomorphism (6).

[§]Strictly speaking, we need to express the entire closed-loop dynamics in terms of error coordinates. Rewriting $\mathcal{M}_x(\mathbf{q}_u) = \mathcal{M}_x(\mathbf{h}_1^{-1}(\tilde{\mathbf{y}} + \mathbf{y}_d(t)))$ and $\mathcal{C}_x(\mathbf{q}_u, \dot{\mathbf{q}}_u) = \mathcal{C}_x(\mathbf{h}_1^{-1}(\tilde{\mathbf{y}} + \mathbf{y}_d(t)), \frac{d}{dt}\mathbf{h}_1^{-1}(\tilde{\mathbf{y}} + \mathbf{y}_d(t)))$ reveals the nonautonomous nature of the closed-loop dynamics. Further, we have $\mathcal{K}_v(\mathbf{q}_u) = \mathcal{K}_v(\mathbf{h}_1^{-1}(\tilde{\mathbf{y}} + \mathbf{y}_d(t)))$. However, we refrain from using this formalism as it would severely affect readability.

[¶]Adopting the core idea behind the strict Lyapunov function in Reference 47 requires diagonal gain matrices.

[#]Note that the skew-symmetry property is system inherent and, thus, independent of the coordinates being used to express the dynamics. Hence, it still holds after transforming the equations of motion into the task space.

ORCID

Manuel Keppler  <https://orcid.org/0000-0002-1532-963X>

REFERENCES

- Uebel M, Minis I, Cleary K. Improved computed torque control for industrial robots. Proceedings of the 1992 IEEE International Conference on Robotics and Automation; 1992:528–533.
- Takegaki M, Arimoto S. A new feedback method for dynamic control of manipulators. *J Dyn Syst Meas Control*. 1981;103(2):119.

3. Khatib O. A unified approach for motion and force control of robot manipulators: the operational space formulation. *IEEE J Robot Autom.* 1987;RA-3(1):43-53.
4. Koditschek D. Natural motion for robot arms. Proceedings of the 23rd IEEE Conference on Decision and Control; 1984:733-735.
5. Paden B, Panjand R. Globally asymptotically stable 'PD+' controller for robot manipulators. *Int J Control.* 1988;47(6):1697-1712.
6. Slotine JE. Putting physics in control-the example of robotics. *IEEE Control Syst Mag.* 1988;8(6):12-18.
7. Alami R, Albu-Schäffer A, Bicchi A, et al. Safe and dependable physical human-robot interaction in anthropic domains: state of the art and challenges. Proceedings of the 2006 IEEE/RSJ International Conference on Intelligent Robots and Systems; 2006:1-16.
8. Tonietti G, Schiavi R, Bicchi A. Design and control of a variable stiffness actuator for safe and fast physical human/robot interaction. Proceedings of the 2005 IEEE International Conference on Robotics and Automation; 2005:526-531.
9. Pratt GA, Williamson MM. Series elastic actuators. Proceedings of the 1995 IEEE/RSJ International Conference on Intelligent Robots and Systems. Human Robot Interaction and Cooperative Robots; Vol. 1, 1995:399-406; IEEE.
10. Hutter M, Gehring C, Jud D, et al. ANYmal - a highly mobile and dynamic quadrupedal robot. Proceedings of the 2016 IEEE/RSJ International Conference on Intelligent Robots and Systems (IROS); 2016:38-44; IEEE.
11. Grebenstein M, Albu-Schäffer A, Bahls T, et al. The DLR hand arm system. Proceedings of the 2011 IEEE International Conference on Robotics and Automation; 2011:3175-3182.
12. Vanderborght B, Albu-Schäffer A, Bicchi A, et al. Variable impedance actuators: a review. *Robot Auton Syst.* 2013;61(12):1601-1614.
13. Ott C. *Cartesian Impedance Control of Redundant and Flexible-Joint Robots*. Springer; 2008.
14. Ott C, Albu-Schäffer A, Kugi A, Hirzinger G. Decoupling based Cartesian impedance control of flexible joint robots. Proceedings of the 2003 IEEE International Conference on Robotics and Automation; Vol. 3, 2003:3101-3107.
15. Khalil HK. *Nonlinear Systems*. 3rd ed. Prentice Hall; 2001.
16. Brogliato B, Ortega R, Lozano R. Global tracking controllers for flexible-joint manipulators: a comparative study. *Automatica.* 1995;31(7):941-956.
17. Spong MW. Modeling and control of elastic joint robots. *Trans ASME J Dyn Syst Measur Control.* 1987;109:310-319.
18. Nicosia S, Tomei P. On the feedback linearization of robots with elastic joints. Proceedings of the 27th IEEE Conference on Decision and Control; 1988:180-185.
19. De Luca A. Dynamic control of robots with joint elasticity. Proceedings of the 1988 IEEE International Conference on Robotics and Automation; 1988:152-158.
20. Palli G, Melchiorri C, De Luca A. On the feedback linearization of robots with variable joint stiffness. Proceedings of the 2008 IEEE International Conference on Robotics and Automation; 2008:1753-1759.
21. De Luca A, Lucibello P. A general algorithm for dynamic feedback linearization of robots with elastic joints. IEEE International Conference on Robotics and Automation; Vol. 1, 1998:504-510; Barcelona, Spain.
22. Della Santina C, Bianchi M, Grioli G, et al. Controlling soft robots: balancing feedback and feedforward elements. *IEEE Robot Automat Mag.* 2017;24(3):75-83.
23. De Luca A, Flacco F. Dynamic gravity cancellation in robots with flexible transmissions. Proceedings of the 2010 49th IEEE Conference on Decision and Control (CDC); 2010:288-295; IEEE.
24. De Luca A, Flacco F. A PD-type regulator with exact gravity cancellation for robots with flexible joints. Proceedings of the 2011 IEEE International Conference on Robotics and Automation; 2011:317-323.
25. Bloch AM, Leonard NE, Marsden JE. Controlled Lagrangians and the stabilization of mechanical systems. I. The first matching theorem. *IEEE Trans Automat Contr.* 2000;45(12):2253-2270.
26. Bloch AM, Chang DE, Leonard NE, Marsden JE. Controlled Lagrangians and the stabilization of mechanical systems. II. Potential shaping. *IEEE Trans Automat Contr.* 2001;46(10):1556-1571.
27. Ortega R, Spong MW, Gomez-Estern F, Blankenstein G. Stabilization of a class of underactuated mechanical systems via interconnection and damping assignment. *IEEE Trans Automat Contr.* 2002;47(8):1218-1233.
28. Keppler M, Lakatos D, Ott C, Albu-Schäffer A. A passivity-based approach for trajectory tracking and link-side damping of compliantly actuated robots. Proceedings of the 2016 IEEE International Conference on Robotics and Automation (ICRA); 2016:1079-1086.
29. Keppler M, Lakatos D, Ott C, Albu-Schäffer A. A passivity-based controller for motion tracking and damping assignment for compliantly actuated robots. Proceedings of the 2016 IEEE 55th Conference on Decision and Control (CDC); 2016:1521-1528; IEEE.
30. Keppler M, Lakatos D, Ott C, Albu-Schäffer A. Elastic structure preserving (ESP) control for compliantly actuated robots. *IEEE Trans Robot.* 2018;34(2):317-335.
31. Keppler M, Lakatos D, Ott C, Albu-Schäffer A. Elastic structure preserving impedance (ESPi) control for compliantly actuated robots. Proceedings of the 2018 IEEE/RSJ International Conference on Intelligent Robots and Systems (IROS); 2018:5861-5868.
32. Van der Schaft AJ. *L2 Gain and Passivity Techniques in Nonlinear Control*. 3rd ed. Springer; 2017.
33. Ortega R. *Passivity-Based Control of Euler-Lagrange Systems: Mechanical, Electrical, and Electromechanical Applications*. Springer; 1998.
34. Pozharitskii G. On asymptotic stability of equilibria and stationary motions of mechanical systems with partial dissipation. *J Appl Math Mech.* 1961;25(4):979-993.
35. Bui HD. Duality and symmetry lost in solid mechanics. *Comptes Rendus Mécanique.* 2008;336(1):12-23. Duality, inverse problems and nonlinear problems in solid mechanics.
36. Ortega R, Van Der Schaft A, Maschke B, Escobar G. Interconnection and damping assignment passivity-based control of port-controlled Hamiltonian systems. *Automatica.* 2002;38(4):585-596.

37. Goldstein H, Poole C, Safko J. *Classical Mechanics*. AAPT; 2002.
38. Nicosia S, Tomei P. A method to design adaptive controllers for flexible joint robots. Proceedings 1992 IEEE International Conference on Robotics and Automation; 1992:701-706.
39. Keppler M, Lakatos D, Werner A, Loeffl F, Ott C, Albu-Schäffer A. Visco-elastic structure preserving impedance (VESPi) control for compliantly actuated robots. Proceedings of the 2018 European Control Conference (ECC); 2018:255-260.
40. Keppler M, Loeffl F, Wandinger D, Raschel C, Ott C. Analyzing the performance limits of articulated soft robots based on the ESPi framework: applications to damping and impedance control. *IEEE Robot Automat Lett*. 2021;6(4):7121-7128.
41. Lanczos C. *The Variational Principles of Mechanics*. Courier Corporation; 2012.
42. Ferrario C, Passerini A. Transformation properties of the Lagrange function. *Revista Brasileira de Ensino de Física*. 2008;30(3):3306.
43. Tomei P. A simple PD controller for robots with elastic joints. *IEEE Trans Automat Contr*. 1991;36(10):1208-1213.
44. Albu-Schäffer A, Ott C, Hirzinger G. Constructive energy shaping based impedance control for a class of underactuated Euler-Lagrange systems. Proceedings of the 2005 IEEE International Conference on Robotics and Automation; 2005:1387-1393; IEEE.
45. Loria A, Ortega R. On tracking control of rigid and flexible joints robots. *Appl Math Comput Sci*. 1995;5(2):101-113.
46. Slotine JJ, Weiping L. Adaptive manipulator control: a case study. *IEEE Trans Automat Contr*. 1988;33(11):995-1003.
47. Spong MW, Ortega R, Kelly R. Comments on "Adaptive manipulator control: a case study" by J. Slotine and W. Li. *IEEE Trans Automat Contr*. 1990;35(6):761-762.
48. Byrnes CI, Isidori A, Willems JC. Passivity, feedback equivalence, and the global stabilization of minimum phase nonlinear systems. *IEEE Trans Automat Contr*. 1991;36(11):1228-1240.
49. Khalil W, Dombre E. *Modeling, Identification and Control of Robots*. 3rd ed. Taylor & Francis, Inc; 2002.
50. Hahn W. *Stability of Motion*. Springer; 1967.
51. Slotine JJE, Li W. On the adaptive control of robot manipulators. *Int J Robot Res*. 1987;6(3):49-59.
52. Rouche N, Habets P, Laloy M. *Stability Theory by Liapunov's Direct Method*. Springer; 1977.

How to cite this article: Keppler M, Ott C, Albu-Schäffer A. From underactuation to quasi-full actuation: Aiming at a unifying control framework for articulated soft robots. *Int J Robust Nonlinear Control*. 2022;32(9):5453-5484. doi: 10.1002/rnc.6102

APPENDIX A. SUPPLEMENTARY MATERIAL

A.1 A detailed derivation of the input transformation

Starting with the robot model (4), and using the state transformation (39), we aim for an input transformation that results in the dynamics (42) with a preserved EL structure. Deriving the state transformation relation (39) with respect to time gives

$$\tau_{\varphi}(\varphi)\dot{\varphi} = \tau_{\varphi}(\tilde{\varphi})\dot{\tilde{\varphi}} + \dot{\bar{u}}_1. \quad (\text{A1})$$

We can solve this equation for the motor velocities

$$\dot{\theta} = \dot{q}_u + \mathbf{A}\dot{\varphi} + \tau_{\varphi}(\varphi)^{-1}\dot{\bar{u}}_1, \quad (\text{A2})$$

with $\mathbf{A}(\varphi, \tilde{\varphi}) = \tau_{\varphi}(\varphi)^{-1}\tau_{\varphi}(\tilde{\varphi})$. Matrix $\tau_{\varphi}(\varphi)$ is invertible due to the assumptions on the elastic potential \mathcal{V}_e . Note that we can rewrite \mathbf{A} as a function of the deflection states and new inputs via (39), that is, with some abuse of notation, $\mathbf{A} = \mathbf{A}(\varphi, \bar{u}_1)$. For linear springs, \mathbf{A} degenerates to a unity matrix which significantly simplifies the input transformation.

Remark 7. In general, we may always replace all occurrences of $\tilde{\varphi}$ and $\dot{\tilde{\varphi}}$ via (39) and (A1) such that the resulting expression is solely a function of the original states \mathbf{z} and the new inputs \bar{u}_1 .

Inserting (39) and (A2) into the second equation of (4) gives

$$\mathbf{B} \left(\ddot{q}_u + \mathbf{A}\ddot{\varphi} + \dot{\mathbf{A}}\dot{\varphi} + \frac{d}{dt} \left(\tau_{\varphi}(\varphi)^{-1}\dot{\bar{u}}_1 \right) \right) + \tau(\tilde{\varphi}) + \bar{u}_1 = \mathbf{u} + Q_{\text{ext},2}. \quad (\text{A3})$$

Exploiting the diagonal nature of \mathbf{B} and \mathbf{A} , we can rewrite (A3) as

$$\mathbf{B}\mathbf{A}(\ddot{q}_u + \ddot{\varphi}) + \mathbf{B}\mathbf{A}\mathbf{B}^{-1}\tau(\tilde{\varphi}) = \mathbf{u} + Q_{\text{ext},2} - \Gamma, \quad (\text{A4})$$

with

$$\Gamma(\mathbf{z}, \dot{\mathbf{z}}, \bar{\mathbf{u}}_1, \dot{\bar{\mathbf{u}}}_1, \ddot{\bar{\mathbf{u}}}_1) = \bar{\mathbf{u}}_1 + \mathbf{B} \left(\dot{\mathbf{A}} \tilde{\boldsymbol{\varphi}} + \frac{d}{dt} \left(\boldsymbol{\tau}_{\boldsymbol{\varphi}}(\boldsymbol{\varphi})^{-1} \dot{\bar{\mathbf{u}}}_1 \right) \right) + (\mathbf{I} - \mathbf{A}) (\mathbf{B} \ddot{\boldsymbol{\varphi}} + \boldsymbol{\tau}(\tilde{\boldsymbol{\varphi}})). \quad (\text{A5})$$

Premultiplying (A4) with $\mathbf{B}\mathbf{A}^{-1}\mathbf{B}^{-1} = \mathbf{A}^{-1}$, we get

$$\mathbf{B} (\ddot{\boldsymbol{q}}_u + \ddot{\boldsymbol{\varphi}}) + \boldsymbol{\tau}(\tilde{\boldsymbol{\varphi}}) = \mathbf{A}^{-1} (\mathbf{u} - \Gamma + \mathcal{Q}_{\text{ext},2}). \quad (\text{A6})$$

Substituting the input transformation

$$\mathbf{u} = \mathbf{A}(\boldsymbol{\varphi}, \tilde{\boldsymbol{\varphi}}) \bar{\mathbf{u}}_2 + \Gamma(\mathbf{z}, \dot{\mathbf{z}}, \bar{\mathbf{u}}_1, \dot{\bar{\mathbf{u}}}_1, \ddot{\bar{\mathbf{u}}}_1) \quad (\text{A7})$$

into (A6), combining the resulting dynamics with the first equation of (4), and taking the state transformation (39) into account gives

$$\begin{bmatrix} \mathbf{M} & \mathbf{0} \\ \mathbf{B} & \mathbf{B} \end{bmatrix} \begin{bmatrix} \ddot{\boldsymbol{q}}_u \\ \ddot{\boldsymbol{\varphi}} \end{bmatrix} + \begin{bmatrix} \mathbf{C} & \mathbf{0} \\ \mathbf{0} & \mathbf{0} \end{bmatrix} \begin{bmatrix} \dot{\boldsymbol{q}}_u \\ \dot{\boldsymbol{\varphi}} \end{bmatrix} + \begin{bmatrix} -\boldsymbol{\tau}(\tilde{\boldsymbol{\varphi}}) \\ \boldsymbol{\tau}(\tilde{\boldsymbol{\varphi}}) \end{bmatrix} + \begin{bmatrix} \mathbf{g}(\mathbf{q}_u) \\ \mathbf{0} \end{bmatrix} = \begin{bmatrix} \bar{\mathbf{u}}_1 \\ \bar{\mathbf{u}}_2 \end{bmatrix} + \mathcal{Q}_{\text{ext}}^*, \quad (\text{A8})$$

where the external forces are scaled according to $\mathcal{Q}_{\text{ext}}^{*\top} \triangleq \begin{bmatrix} \mathcal{Q}_{\text{ext},1}^T & (\mathbf{A}^{-1} \mathcal{Q}_{\text{ext},2})^T \end{bmatrix}$. We finish the transformation by premultiplying equation (A8) with \mathbf{T}_z^{-T} to obtain the desired form (42).

Remark 8. By introducing virtual motor states

$$\tilde{\boldsymbol{q}}_a \triangleq \tilde{\boldsymbol{\varphi}} + \mathbf{q}_u \quad (\text{A9})$$

and inserting this relation into (A8), we would obtain the quasi-fully actuated form in terms of the virtual motor-states

$$\begin{bmatrix} \mathbf{M} & \mathbf{0} \\ \mathbf{0} & \mathbf{B} \end{bmatrix} \begin{bmatrix} \ddot{\boldsymbol{q}}_u \\ \ddot{\boldsymbol{q}}_a \end{bmatrix} + \begin{bmatrix} \mathbf{C} & \mathbf{0} \\ \mathbf{0} & \mathbf{0} \end{bmatrix} \begin{bmatrix} \dot{\boldsymbol{q}}_u \\ \dot{\boldsymbol{q}}_a \end{bmatrix} + \begin{bmatrix} -\boldsymbol{\tau}(\tilde{\boldsymbol{\varphi}}) \\ \boldsymbol{\tau}(\tilde{\boldsymbol{\varphi}}) \end{bmatrix} + \begin{bmatrix} \mathbf{g}(\mathbf{q}_u) \\ \mathbf{0} \end{bmatrix} = \begin{bmatrix} \bar{\mathbf{u}}_1 \\ \bar{\mathbf{u}}_2 \end{bmatrix} + \mathcal{Q}_{\text{ext}}^*. \quad (\text{A10})$$

Some concepts in this article can be understood easier in terms of the virtual deflection states and some in terms of the virtual motor states. In particular, thinking in terms of virtual motor states allows for a more intuitive understanding of the feedforward and damping terms implemented via the second input $\bar{\mathbf{u}}_2$ in Section 5.

A.2 Theorems and propositions

Consider the dynamics system

$$\dot{\mathbf{x}} = \mathbf{f}(t, \mathbf{x}), \quad (\text{A11})$$

where $\mathbf{x} \in \mathbb{R}^n$, $t \in \mathbb{R}$ is the time and \mathbf{f} is a continuous function $\mathbf{f} : I \times \Omega \rightarrow \mathbb{R}^n$, where $I = [t_0, \infty)$ for some $t_0 \in \mathbb{R}$ and Ω is an open connected set in \mathbb{R}^n , containing the origin. We assume that $\mathbf{f}(t, \mathbf{0}) = \mathbf{0} \forall t \in I$, so that the origin is an equilibrium point for the differential equation (A11). Matrosov's theorem then states:

Matrosov's Theorem (52). *Let there exist two C^1 functions $V : I \times \Omega \rightarrow \mathbb{R}$, $W : I \times \Omega \rightarrow \mathbb{R}$, a C^0 function $V^* : \Omega \rightarrow \mathbb{R}$, three functions a, b, c of class \mathcal{K} and two constants $S > 0$ and $T > 0$ such that, for every $(t, \mathbf{x}) \in I \times \Omega$*

1. $a(|\mathbf{x}|) \leq V(t, \mathbf{x}) \leq b(|\mathbf{x}|)$;
2. $\dot{V}(t, \mathbf{x}) \leq V^*(\mathbf{x}) \leq 0$; $E \triangleq \{\mathbf{x} \in \Omega : V^*(\mathbf{x}) = 0\}$;
3. $|W(t, \mathbf{x})| < S$;
4. $\max(d(\mathbf{x}, E), |\dot{W}(t, \mathbf{x})|) \geq c(|\mathbf{x}|)$;
5. $|\mathbf{f}(t, \mathbf{x})| < T$;

choosing $\alpha > 0$ such that $\bar{B}_\alpha \subset \Omega$, let us put for every $t \in I$

$$V_{t,\alpha}^{-1} = \mathbf{x} \in \Omega : V(t, \mathbf{x}) \leq a(\alpha). \quad (\text{A12})$$

Then

1. for any $t_0 \in I$ and any $\mathbf{x}_0 \in V_{t_0, \alpha}^{-1}$, any solution $\mathbf{x}(t)$ of (A11), passing through $(\mathbf{x}_0, t_0) \in I \times \Omega$, tends to zero uniformly in t_0 and \mathbf{x}_0 , as $t \rightarrow \infty$.
2. the origin is uniformly asymptotically stable.

Above, $d(\mathbf{x}, E)$ denotes the minimum distance of point \mathbf{x} to set E , that is, $\inf_{y \in E} (||\mathbf{x} - \mathbf{y}||)$. In order to facilitate the verification of Matrosov's condition (4), we apply the following lemma by Paden and Panja:

Lemma 1 (5). Condition (4) of Matrosov's theorem is satisfied if conditions below are satisfied.

- (iv.a) $\dot{W}(\mathbf{x}, t)$ is continuous in both arguments and depends on time in the following way. $\dot{W}(\mathbf{x}, t) = g(\mathbf{x}, \beta(t))$ where g is continuous in both of its arguments. $\beta(t)$ is also continuous and its image lies in a bounded set K_1 . (For simplicity, we assume that $\dot{W}(\mathbf{x}, t)$ depends on time continuously through a bounded function.)
- (iv.b) There exists a class \mathcal{K} function, k , such that $|\dot{W}(\mathbf{x}, t)| \geq k(||\mathbf{x}||) \forall \mathbf{x} \in E$ and $t \geq t_0$.

Proposition 3 (33, p. 28). The equilibria of a fully damped unforced EL system (i.e., with $\mathbf{u} = Q_{\text{ext}} = \mathbf{0}$) are $(\mathbf{q}, \dot{\mathbf{q}}) = (\mathbf{q}_d, \mathbf{0})$, where \mathbf{q}_d is the solution of

$$\frac{\partial \mathcal{V}}{\partial \dot{\mathbf{q}}}(\mathbf{q}) = \mathbf{0}. \quad (\text{A13})$$

The equilibrium is stable if \mathbf{q}_d is a strict local minimum of the potential energy function $\mathcal{V}(\mathbf{q})$. Furthermore, if $\mathcal{V}(\mathbf{q})$ is proper and the minimum is unique, then this equilibrium is GAS.

A.3 Important relations and definitions

The original inertia matrix \mathcal{M} and Coriolis/centrifugal matrix C transformed into the deflection space are given by

$$\mathcal{M}_z(\mathbf{q}_u) = \begin{bmatrix} \mathbf{M}(\mathbf{q}_u) + \mathbf{B} & \mathbf{B} \\ \mathbf{B} & \mathbf{B} \end{bmatrix}, \quad C_z(\mathbf{q}_u, \dot{\mathbf{q}}_u) = \begin{bmatrix} \mathbf{C}(\mathbf{q}_u, \dot{\mathbf{q}}_u) & \mathbf{0} \\ \mathbf{0} & \mathbf{0} \end{bmatrix}.$$

Their transformations into the task space are given by

$$\mathcal{M}_x = \mathbf{T}_x^{-\text{T}} \mathbf{T}_z^{-\text{T}} \begin{bmatrix} \mathbf{M} & \mathbf{0} \\ \mathbf{0} & \mathbf{B} \end{bmatrix} \mathbf{T}_z^{-1} \mathbf{T}_x^{-1} = \begin{bmatrix} \mathbf{J}^{-\text{T}}(\mathbf{q}_u) (\mathbf{M}(\mathbf{q}_u) + \mathbf{B}) \mathbf{J}^{-1}(\mathbf{q}_u) & \mathbf{J}^{-\text{T}}(\mathbf{q}_u) \mathbf{B} \\ \mathbf{B} \mathbf{J}^{-1}(\mathbf{q}_u) & \mathbf{B} \end{bmatrix}$$

and

$$C_x \triangleq \begin{bmatrix} \mathbf{J}^{-\text{T}}(\mathbf{q}_u) (\mathbf{M}(\mathbf{q}_u) + \mathbf{B}) \mathbf{J}^{-1}(\mathbf{q}_u) + \mathbf{J}^{-\text{T}}(\mathbf{q}_u) \mathbf{C}(\mathbf{q}_u, \dot{\mathbf{q}}_u) \mathbf{J}^{-1}(\mathbf{q}_u) & \mathbf{0} \\ \mathbf{B} \mathbf{J}^{-1} & \mathbf{0} \end{bmatrix}.$$

In these expressions we can identify the transformed link-side inertia and Coriolis/centrifugal matrices

$$\mathbf{M}_y(\mathbf{q}_u) \triangleq \mathbf{J}^{-\text{T}}(\mathbf{q}_u) \mathbf{M}(\mathbf{q}_u) \quad (\text{A14})$$

and

$$\mathbf{C}_y(\mathbf{q}_u, \dot{\mathbf{q}}_u) \triangleq \mathbf{J}^{-\text{T}}(\mathbf{q}_u) \mathbf{M}(\mathbf{q}_u) \mathbf{J}^{-1}(\mathbf{q}_u) + \mathbf{J}^{-\text{T}}(\mathbf{q}_u) \mathbf{C}(\mathbf{q}_u, \dot{\mathbf{q}}_u) \mathbf{J}^{-1}(\mathbf{q}_u). \quad (\text{A15})$$

The structure preserving input and state transformation of Section 3 transforms the generalized external forces Q_{ext} as

$$Q_{\text{ext}}^* = \begin{bmatrix} \mathbf{I} & \mathbf{0} \\ \mathbf{0} & \mathbf{A}^{-1} \end{bmatrix} Q_{\text{ext}}. \quad (\text{A16})$$

Transformation and input matrices

$$\begin{aligned} \mathbf{T}_z &= \begin{bmatrix} \mathbf{I} & \mathbf{0} \\ -\mathbf{I} & \mathbf{I} \end{bmatrix}; & \mathbf{T}_x &= \begin{bmatrix} \mathbf{J}(\mathbf{q}_u) & \mathbf{0} \\ \mathbf{0} & \mathbf{I} \end{bmatrix}; & \mathcal{N}_{\bar{z}} &= \mathbf{T}_z^{-T} = \begin{bmatrix} \mathbf{I} & \mathbf{I} \\ \mathbf{0} & \mathbf{I} \end{bmatrix}; & \mathcal{N}_x &= \mathbf{T}_x^{-T} \mathbf{T}_z^{-T} = \begin{bmatrix} \mathbf{J}^{-T}(\mathbf{q}_u) & \mathbf{J}^{-T}(\mathbf{q}_u) \\ \mathbf{0} & \mathbf{I} \end{bmatrix}; \\ \mathbf{T}_z^{-1} &= \begin{bmatrix} \mathbf{I} & \mathbf{0} \\ \mathbf{I} & \mathbf{I} \end{bmatrix}; & \mathbf{T}_x^{-1} &= \begin{bmatrix} \mathbf{J}^{-1}(\mathbf{q}_u) & \mathbf{0} \\ \mathbf{0} & \mathbf{I} \end{bmatrix}; & \mathcal{N}_{\bar{z}}^{-1} &= \begin{bmatrix} \mathbf{I} & -\mathbf{I} \\ \mathbf{0} & \mathbf{I} \end{bmatrix}; & \mathcal{N}_x^{-1} &= \begin{bmatrix} \mathbf{J}^T(\mathbf{q}_u) & -\mathbf{I} \\ \mathbf{0} & \mathbf{I} \end{bmatrix}; & \mathcal{N}_z &= \begin{bmatrix} \mathbf{0} & \mathbf{0} \\ \mathbf{0} & \mathbf{I} \end{bmatrix}; \end{aligned}$$

Gain matrices

Expression (59) can be expanded as

$$\mathcal{K}_v(\mathbf{q}_u) = \mathbf{T}_x^{-T} \mathbf{T}_z^{-T} \mathbf{T}_x^T \begin{bmatrix} \mathcal{K}_{v,1} & \mathbf{0} \\ \mathbf{0} & \mathcal{K}_{v,2} \end{bmatrix} \mathbf{T}_x \mathbf{T}_z^{-1} \mathbf{T}_x^{-1} = \begin{bmatrix} \mathcal{K}_{v,1} + \mathbf{J}^{-T}(\mathbf{q}_u) \mathcal{K}_{v,2} \mathbf{J}^{-1}(\mathbf{q}_u) & \mathbf{J}^{-T}(\mathbf{q}_u) \mathcal{K}_{v,2} \\ \mathcal{K}_{v,2} \mathbf{J}^{-1}(\mathbf{q}_u) & \mathcal{K}_{v,2} \end{bmatrix}$$

Note the structural analogy to how the original inertia matrix transforms into task space, compare \mathcal{M}_x . Note that we defined the gain matrix $\mathcal{K}_{v,1}$ for the rigid coordinates already in task space.